1 # Eddy-enhanced primary production sustains heterotrophic microbial
2 # activities in the Eastern Tropical North Atlantic

3 Quentin Devresse[1], Kevin W. Becker[1], Arne Bendinger[1,2], Johannes Hahn[1,3], Anja Engel[1]

4 [1]GEOMARHelmholtz Centre for Ocean Research Kiel, Germany,

5 [2]Laboratoire d'Etudes en Géophysique et Océanographie Spatiales (LEGOS), Université Toulouse,

6 IRD, CNRS, CNES, UPS, Toulouse, France

7 [3]Bundesamt für Seeschifffahrt und Hydrographie, Hamburg, Germany

9 Correspondence: Quentin Devresse (qdevresse@geomar.de)

Abstract

12 Mesoscale eddies modulate the ocean's physical, chemical, and biological properties. In
13 cyclonic eddies (CE), nutrient upwelling can stimulate primary production by phytoplankton.
14 Yet, how this locally enhanced autotrophic production affects heterotrophy and consequently
15 the metabolic balance between the synthesis and the consumption of dissolved organic matter
16 (DOM) remains largely unknown. To fill this gap, we investigated the horizontal and vertical
17 variability of auto- and heterotrophic microbial activity (biomass production and respiration)
18 within a CE that formed off Mauritania and along the ~900 km zonal corridor between
19 Mauritania and the Cape Verde Islands in the eastern tropical North Atlantic (ETNA). Our
20 results show how the physical disturbances caused by the CE affected the biomass distribution
21 of phyto- and bacterioplankton and their metabolic activities.. The injection of nutrients into
22 the sunlit surface resulted in enhanced autotrophic pico- and nanoplankton abundance and
23 generally increased autotrophic activity as indicated by Chlorophyll a (Chl-a) concentration,
24 primary production (PP) and extracellular release rates. However, the detailed eddy survey
25 also revealed an uneven distribution of these variables with, for example, the highest Chl-a
26 concentrations and PP rates occurring near and just beyond the CE's periphery. The
27 heterotrophic bacterial activity was similarly variable. Optode-based community respiration
28 (CR) bacterial respiration (BR) estimates and bacterial biomass production (BP) largely
29 followed the trends of PP and Chl-a. Thus, a submesoscale spatial mosaic of heterotrophic
30 bacterial abundance and activities occurred within the CE that was closely related to variability
31 in autotrophic production. Consistent with this, we found a significant positive correlation

between concentrations of semi-labile dissolved organic carbon (SL-DOC; here the sum of dissolved hydrolyzable amino acids and dissolved combined carbohydrates) and BR estimates. Extracellular release of carbon as indicated by primary production of dissolved organic carbon (PP_{DOC}) was variable with depth and laterally and not always sufficient to compensate the bacterial carbon demand (BCD: BR+BP) with PP_{DOC} accounting between 28% and 110% of the BCD. Bacterial growth efficiency (BGE: BP/BCD) ranged between 1.7 and 18.2%. We estimated the metabolic state to establish whether the CE was a source or a sink of organic carbon. We showed that the CE carried a strong autotrophic signal in the core (PP/CR>1). Our results suggest that submesoscale (0-10 km) processes lead to highly variable metabolic activities of both photoautotrophic and heterotrophic microorganisms. Overall, we revealed that the CEs not only trap and transport coastal nutrients and organic carbon to the open ocean, but also stimulate phytoplankton growth generating freshly produced organic matter during westward propagation. This drives heterotrophic processes and may contribute to the previously observed net heterotrophy in open Atlantic surface waters.

1. Introduction

Mesoscale eddies (10-100 km) are ubiquitous in the ocean affecting upper ocean biogeochemistry and ecology. For example, upwelling of nutrients inside eddies can enhance primary production and carbon export (Cheney and Richardson, 1976; Arístegui et al., 1997). The sense of rotation and their vertical structure classifies cyclonic (CEs), anticyclonic (ACEs; e.g., Chelton et al., 2011) or anticyclonic mode water eddies (ACMEs; D'Asaro 1988). In Eastern Boundary Upwelling Systems (EBUS), eddies typically form by flow separation along slope boundary currents at topographic headlands (D'Asaro, 1988; Molemaker et al., 2015; Thomsen et al., 2016). Eddies have lifespans from days to months and can travel several hundred to thousands of kilometers across ocean basins (Chelton et al., 2011). In the North Atlantic Ocean, eddies generated in the highly productive Canary Upwelling System (CanUS) may laterally propagate to the oligotrophic Subtropical North Atlantic Gyre (SNAG), transporting nutrients and carbon from the coast to the open ocean (McGillicuddy et al., 2003; Karstensen et al., 2015; Schütte et al., 2016). Various studies demonstrated the impact of eddies on primary production (PP) on a global scale. However, the effects of eddies vary regionally, and studies with higher spatial resolution of eddies combined with advances in *in situ* observation, remote sensing and modelling are still needed to better describe the physical and

biological properties of the upper ocean. (see review by McGillicuddy, 2016 and references therein). For example, Couespel et al. (2021) performed global warming simulations using a representation of mid-latitude double-gyre circulation. They showed that at the finest model resolution (1/27°), eddies can mitigate the decline of primary production (-12 % at 1/27° vs. -26 % at 1°). Modeling studies have long urged consideration of the effects of eddies on PP at submesoscale levels (0.1-10 km) to provide more realistic estimates of the oceanic carbon cycle (Lévy et al., 2001). Eddies modulate the mixed layer depth by upwelling (CEs), downwelling (ACEs), or frontogenesis from eddy-eddy interaction, thereby creating spatial variability of nutrient concentration within and around eddies on the submesoscale (see reviews by Mahadevan, 2016 and McGillicuddy, 2016). In addition, the nonlinear response of phytoplankton growth to nutrient availability and advection of phytoplankton by currents makes plankton distribution and community composition highly variable within and around eddies (Lochte and Pfannkuche 1987). As a consequence, the spatial distribution of PP across eddies can be highly variable (e.g., Falkowski et al., 1991; Ewart et al., 2008; Singh et al., 2015).

Bacterial activity is directly coupled to PP, as autotrophic cells release their main substrate dissolved organic matter (DOM), . DOM release by phytoplankton mainly occurs via two mechanisms: 1) passive leakage of small molecules by diffusion across the cell membrane and 2) active exudation of DOM into the surrounding environment (Engel et al., 2004). Environmental conditions, such as temperature, nutrient availability (e.g., Borchard and Engel, 2012) and light conditions (e.g., Cherrier et al., 2015) affect the amount and the elemental stoichiometry of released DOM. Patchiness of phytoplankton primary productivity and nutrient availability within eddies may thus lead to spatial heterogeneity of extracellular release rates (e.g., Lasternas et al., 2013; Rao et al., 2021) and DOM quality (e.g., Wear et al., 2020). DOM quality impacts bacterial biomass production (BP), bacterial respiration (BR), and bacterial growth efficiency (BGE; e.g., Neijssel and de Mattos, 1994; Russell and Cook, 1995; Robinson, 2008; Lipson, 2015). BGE is the ratio between BP and the bacterial carbon demand (BCD), which is the sum of respired carbon and carbon incorporated into biomass (BP + BR). Lønborg et al. (2011) observed that BGE decreases with increasing C/N ratio of phytoplankton-derived DOM. BGE is a critical parameter for estimating the amount of consumed organic carbon used to build biomass by heterotrophic bacteria (Anderson and Ducklow 2001). So far, BGE has been reported for ACEs from the Mediterranean Sea (Christaki et al., 2021) but not for CEs and ACMEs. In general, several studies showed a patchy distribution of bacterial abundance, BP (Ewart et al., 2008; Baltar et al., 2010), BR (Mouriño-Carballido, 2009; Jiao et al., 2014),

community respiration (CR; Mouriño-Carballido and McGillicuddy, 2006; Mouriño-Carballido, 2009), and of the metabolic balance between the production and consumption of organic matter (Maixandeau et al., 2005; Ewart et al., 2008; Mouriño-Carballido and McGillicuddy, 2006; Mouriño-Carballido, 2009) within eddies. Yet, insights into the distribution of phytoplankton and their activities within mesoscale eddies are limited due to insufficient fine-scale vertical and horizontal resolution studies to adequately describe these distributions. Thus, data on eddy-induced changes in primary production, extracellular release and semi-labile DOM concentration, and the responses of heterotrophic microbial metabolic activities are scarce. Understanding how eddies modulate microbial activities will enhance our knowledge about the fate of organic carbon and the overall CO_2 source/sink function in the ocean, particularly in EBUS, where eddy generation is high (Pegliasco et al., 2015).

Here, we studied the impact of a CE on microbial carbon cycling along a 900 km zonal corridor of the westward propagating eddies between the Cape Verde Islands and the Mauritania Upwelling System (13-20 °N), a sub-region of the CanUS (13-33 °N, Arístegui et al., 2009). About 146 ± 44 eddies with a lifetime of more than 7 days are generated per year in this region (Schütte et al., 2016). Along this corridor, a CE was sampled at high spatial resolution to resolve the heterogeneity of microbial processes at the submesoscale. We determined phytoplankton (<20 μm) cell abundance, primary production, and extracellular release and linked those measurements of autotrophic activity to semi-labile DOM concentration and heterotrophic bacterial activity. Our study provides new insights into 1) microbial carbon cycling and 2) factors controlling microbial metabolic activities within and around CE formed in EBUS.

2. Materials and Methods

2.1 Study area and eddy characterization

Sampling was conducted in the ETNA between the Cape Verde archipelago and the Mauritanian coast during cruise M156 (July 3rd to August 1st, 2019. Figure **1A**) on the R/V *Meteor*. Samples were collected during the relaxation period, which is typically from May to July following the upwelling season (January to March; Lathuilière et al., 2008). A CE was sampled at high spatial resolution along two zonal transects (from 19.1 °W to 18.2 °W at 18.3 °N and from 18.5 °W to 17.1 °W at 18.6 °N) and one meridional transect (from 19.4 °N to 18

°N at 18.4 °W to 18.1 °W). The zonal transect slightly shifted east/west of the eddy core position. The reason for that was the deformed eddy shape (see Fig. **1A**), which made it challenging to identify the center of the eddy and required rerouting of the ship's track during the survey. In addition, we sampled water along an 18 °N transect, a typical coast to open ocean trajectory of eddies in this region (Schütte et al., 2016). Salinity, temperature, depth, and O_2 concentration were determined using a Seabird 911 plus CTD system equipped with two independently working sets of temperature-conductivity-oxygen sensors. The oxygen sensor was calibrated against discrete water samples using the Winkler method (Strickland and Parsons, 1968; Wilhelm, 1888). Seawater samples were collected using 10 L Niskin bottles attached to the CTD Rosette. A total of 25 stations (**SI Table S1**) were sampled, 14 of them inside or in the vicinity of the CE. Sampling was conducted in the epipelagic layer (0-200 m), including samples from the surface mixed layer, the Chl-*a* maximum, and the shallow oxygen minimum zone (OMZ; <50 µmol kg^{-1} between 0-200 m depth) when present.

Sea surface height (SSH) and Acoustic Doppler Current Profiler (ADCP) velocity data (SI Fig. **1**) characterized the eddy as a CE. Based on the Angular Momentum Eddy Detection and Tracking Algorithm (AMEDA; Le Vu et al., 2018), the eddy was estimated to be 1.5 months old. The center of the eddy and the core radius were determined using ADCP reconstructions assuming an axis-symmetric vortex. (SI Fig. **1**). On July 22nd 2019, the eddy center was located at 18.69 °N, 18.05 °W, with a core radius of 40.5 ± 5.7 km. The mean azimuthal velocity in the CE was 19.9 ± 0.7 cm s^{-1} and the absolute dynamic topography associated with the CE core was ~23 cm on July 23rd 2019. Fine-scale analysis of the eddy physics will be given by Fischer et al. (2022, in prep). However, as the eddy shape was deformed, ADCP reconstruction did not constrain well the physical border of the eddy (SI Fig. **S1**). Therefore, we combined sea surface temperature (23.44 ± 0.47 °C), salinity (39.95 ± 0.04) and Chl-*a* (1.35 ± 0.73 µg L^{-1}) data to approximate the area influenced by the eddy (Fig. **1b,c,d**). We classified stations into 'core' and 'periphery' of the eddy. Stations that were outside and westward of the eddy influence were referred to as 'open ocean' and those close to the coast as 'coastal'. Just beyond the eddy periphery, at St. E3, a front was observed with surface temperature and salinity (not compensated by density) different from the adjacent stations (Fig. **1b**). Hence, we referred to that station as 'Frontal Zone'. The classification of stations is thoroughly discussed in the supplementary information (SI), and the sampling time, location, and distance from the eddy center are given in SI Table **S1**.
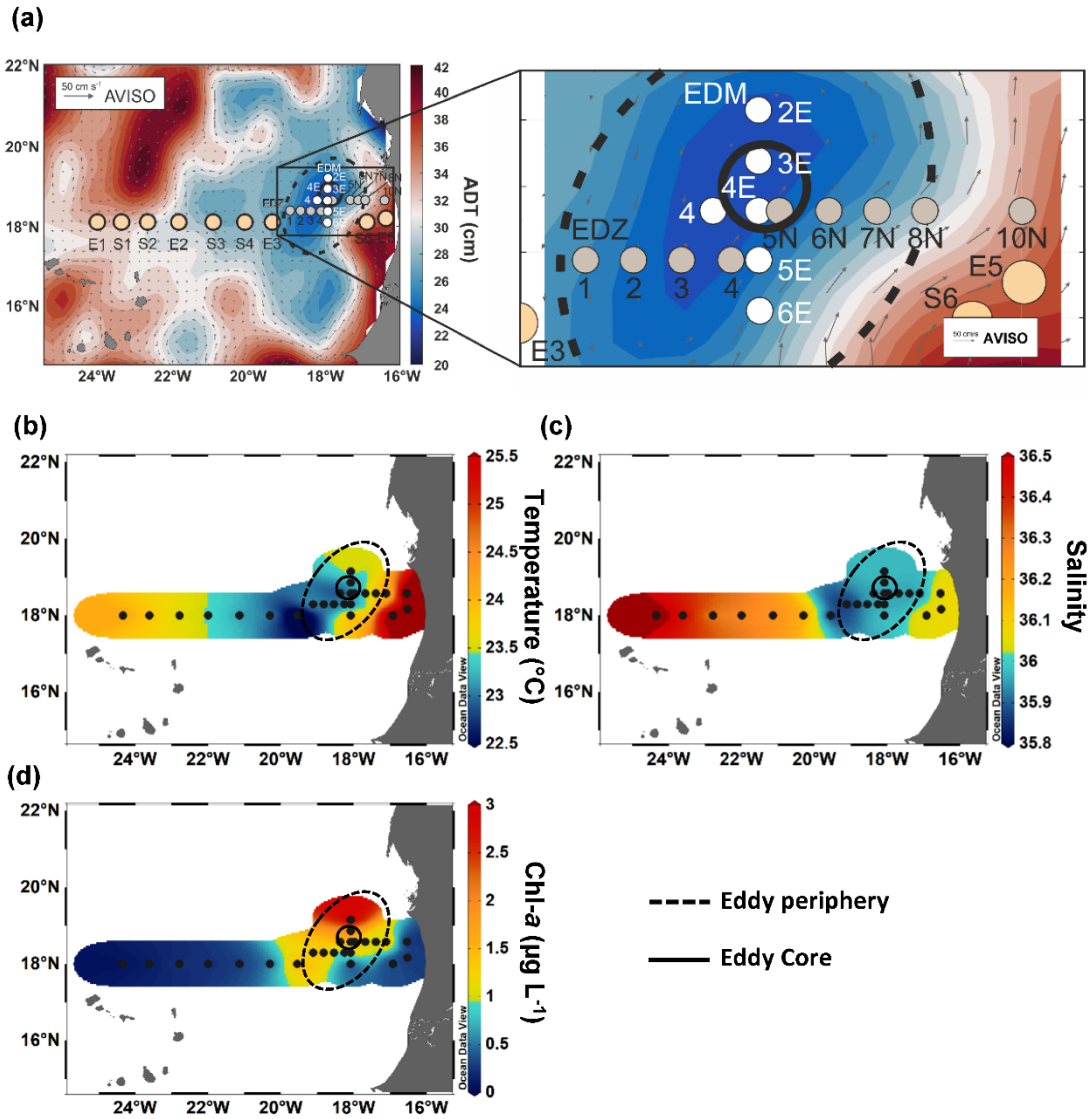
Figure 1: Sampling stations during RV *Meteor* cruise M156 including zoom in into the eddy (**a**), temperature at 5 m depth (**b**), salinity at 5 m depth (**c**), and chlorophyll *a* at 5 m depth (**d**). The background in (**a**) shows the variations in Absolute Dynamic Topography (ADT) obtained from www.aviso.altimetry.fr. The direction and speed of surface water geostrophic currents are shown as arrows. The solid circle in (**a**) – (**d**) indicates the core of the eddy and the dashed circle outlines the periphery.

2.2 Chemical analyses

Nutrient concentrations were determined at selected stations (SI Table **S1**). Nutrients were measured onboard from duplicate unfiltered seawater samples (11 mL). Ammonium (NH_4^+) was analyzed after Solórzano (1969) and phosphate (PO_4), nitrate (NO_3^-), nitrite (NO_2^-), and

176   silicate (Si(OH)$_4$) were measured photometrically with continuous-flow analysis on an auto-

177   analyzer (QuAAtro; Seal Analytical) after Grasshoff et al., (1999). Detection limits for NH$_4^+$,

178   PO$_4$, NO$_3$, NO$_2$, and Si(OH)$_4$ were 0.1, 0.02, 0.1, 0.02, and 0.2 µmol L^{-1}, respectively. Dissolved

179   inorganic nitrogen (DIN) was calculated as the sum of NH$_4^+$, NO$_3^-$, and NO$_2^-$.

180   To estimate the fraction of semi-labile dissolved organic carbon (SL-DOC), we determined

181   high-molecular-weight (HMW > 1 kDa) dissolved combined carbohydrates (dCCHO) and

182   dissolved hydrolysable amino acids (dHAA) as the main biochemical components of DOM

183   (Carlson, 2002). For dCCHO analysis, duplicate samples (20 mL) were filtered through 0.45

184   µm Acrodisk filters, collected in combusted glass vials (8 h, 450 °C) and frozen (-20 °C) until

185   analysis after Engel and Händel (2011) with a detection limit of 1 µg L^{-1}. The analysis detected

186   11 monomers: arabinose, fucose, galactose, galactosamine, galacturonic acid, glucosamine,

187   glucose, glucuronic acid, rhamnose, co-elute mannose, and xylose. For dHAA analysis,

188   duplicate samples (4 mL) were filtered through 0.45 µm Acrodisk filters, collected in

189   combusted glass vials (8 h, 450 °C), and frozen (-20 °C) until analysis. dHAA were measured

190   with ortho- phthaldialdehyde derivatization by high-performance liquid chromatography

191   (HPLC; Agilent Technologies, USA) equipped with a C$_{18}$ column (Phenomenex, USA)

192   (Lindroth and Mopper, 1979; Dittmar et al., 2009). The analysis classified 13 monomers with

193   a precision < 5 % and a detection limit of 2 nmol L^{-1}: alanine, arginine, aspartic acid, isoleucine,

194   glutamic acid, glycine, leucine, phenylalanine, serine, threonine, tyrosine, valine; and γ-

195   aminobutyric acid (GABA). The calculations for the carbon content of dCCHO and dHAA were

196   based on carbon atoms contained in the identified monomers. The sum of dCCHO and dHAA

197   carbon content is referred to as SL-DOC.

198   For Chl-*a,* 1 L seawater samples were filtered onto 25 mm GF/F filters (0,7 µm pore size,

199   Whatman, GE Healthcare Life Sciences, UK) and subsequently frozen (-20 °C) until extraction

200   using 90% acetone for photometric analyses (Turner Designs, USA) slightly modified after

201   Evans et al., (1987).

202   Bacteria were quantified using a flow cytometer (FACSCalibur, Becton Dickinson, Oxford,

203   UK). Seawater samples (1.7 mL) were fixed with 85 µL glutaraldehyde (1% final

204   concentration) and stored at -80 °C until analysis. Samples were stained with SYBR Green I

205   (molecular probes) and enumerated with a laser emitting at 488 nm and detected by their

206   signature in a plot of side scatter (SSC) versus green fluorescence (FL1). Heterotrophic bacteria

207   were distinguished from photosynthetic bacteria (*Prochlorococcus* and *Synechococcus*) by their

208   signature in a plot of red fluorescence (FL2) versus green fluorescence (FL1). Yellow-green

209   latex beads (1 μm, Polysciences) were used as an internal standard (Gasol and del Giorgio,

210   2000). Cell counts were determined with the CellQuest software (Becton Dickinson). For

211   autotrophic pico and nanoplankton <20 μm, 2 mL samples were fixed with formaldehyde (1 %

212   final concentration) and stored frozen (-80 °C) until analysis. Red and orange autofluorescence

213   was used to identify Chl-*a* and phycoerythrin cells. Cell counts were determined with CellQuest

214   software (Becton Dickinson); picoplankton and nanoplankton populations containing Chl-*a*

215   and/or phycoerythrin (i.e., *Synechococcus*) were identified and enumerated. We converted the

216   cell abundance of the different autotrophic pico- and nanoplankton populations into biomass

217   assuming 43 fg C cell^{-1} for *Prochlorococcus*, 120 fg C cell^{-1} for *Synechococcus*, 500 fg C cell^{-1}

218   for eukaryotic picoplankton and, 3.100 fg C cell^{-1} for eukaryotic nanoplankton after

219   Hernández-Hernández et al. (2020). We report the autotrophic pico- and nanoplankton biomass

220   as the sum of eukaryotic pico- and nanoplankton and cyanobacteria (*Prochlorococcus* and

221   *Synechococcus*) biomass. The abundance of eukaryotic pico- and nanoplankton and

222   cyanobacteria (*Prochlorococcus* and *Synechococcus*) can be found in the SI (Table **S2**).

223

224   2.3 Microbial activities

225

226   Primary production (PP) was determined from ^{14}C incorporation according to Steemann

227   Nielsen (1952) and Gargas (1975). Polycarbonate bottles (Nunc EasYFlask, 75 cm^2) were filled

228   with 260 mL prefiltered (mesh size of 200 μm) sample and spiked with 50 μL of a ~11 μCi

229   NaH^{14}CO$_3^-$ solution (Perkin Elmer, Norway). 200 μL were removed immediately after spiking

230   and transferred to a 5 mL scintillation vial for determination of added activity. Then, 50 μL of

231   2N NaOH and 4 mL scintillation cocktail (Ultima Gold AB) were added. Duplicate samples

232   from the top three depths at selected stations (SI Table S**1**) were incubated in 12 h light and 12

233   h dark at 22 °C, which was the average temperature of the upper 100 m depth (22 ± 3°C) along

234   the transect. The incubator was set to reproduce three light levels: 1200-1400; 350 and 5 μE,

235   with high values representing surface irradiance at the time of sampling. The incubation length

236   was chosen for two reasons. First, we expected low productivity of the open ocean

237   phytoplankton community due to low biomass and low nutrient concentrations at the start of

238   the incubation. Under these conditions, short-term incubations of only a few hours may

239   underestimate PP because carbon assimilation by algal cells may be too low to discriminate

240   against ^{14}C adsorption as determined in blank dark incubation (Engel et al., 2013). Moreover,

241   the release of freshly assimilated carbon into the DOM pool has a time scale of several hours

because of the equilibration of the tracer and because metabolic processes of organic carbon exudation follow those of carbon fixation inside the cell (Engel et al., 2013). Incubations were stopped by filtration of a 70 mL sub-sample onto 0.4 μm polycarbonate filters (Nuclepore). Particulate primary production (PP$_{POC}$) was determined from material collected on the filter, while the filtrate was used to determine dissolved primary production (PP$_{DOC}$). All filters were rinsed with 10 mL sterile filtered (<0.2 μm) seawater, and then acidified with 250 μL 2N HCl to remove inorganic carbon (Descy et al., 2002). Filters were transferred into 5 mL scintillation vials, and 4 mL scintillation cocktail (Ultima Gold AB) was added. To determine PP$_{DOC}$, 4 mL of filtrate were transferred to 20 mL scintillation vials and acidified with 100 μL 1N HCl. Scintillation vials were left open in the fume hood for 14 hours to remove inorganic carbon. Then, 100 μL of 2N NaOH and 15 mL scintillation cocktail were added. All samples were counted the following day in a liquid scintillation analyzer (Packard Tri-Carb, model 1900 A).

Primary production (PP) of organic carbon was calculated according to Gargas (1975):

$$\text{PP (μmol C L}^{-1}\text{ d}^{-1}) = \frac{a2 \times DI^{12}C \times 1.05 \times k_1 \times k_2}{a1} \qquad \text{(Eq.1)},$$

where $a1$ and $a2$ are the activities (DPM) (disintegrations per minute) of the added solution and the sample corrected for dark sample, respectively, and DI^{12}C is the concentration (μmol L^{-1}) of dissolved inorganic carbon (DIC) in the sample. DIC concentration was calculated from total alkalinity using the R package seacarb (Gattuso et al., 2020). Total alkalinity of the seawater was acquired through the open-cell titration method (Dickson et al., 2007). The value 1.05 is a correction factor for the discrimination between ^{12}C and ^{14}C, as the uptake of the ^{14}C isotope is 5% slower than the uptake of ^{12}C, k_1 is a correction factor for subsampling (bottle volume/filtered volume) and k_2 is the incubation time (d^{-1}). Total primary production (PP$_{TOT}$; μmol C L^{-1} d^{-1}) was derived from the sum of PP$_{POC}$ and PP$_{DOC}$ according to:

$$PP_{TOT} = \text{PP}_{POC} + \text{PP}_{DOC} \qquad \text{(Eq.2)}$$

The percentage of extracellular release (PER; %) was calculated as:

$$\text{PER} = \left(\frac{\text{PP}_{DOC}}{\text{PP}_{TOT}}\right) \times 100 \qquad \text{(Eq.3)}$$

Bacterial biomass production rates (BP) were measured through the incorporation of labeled leucine (^{3}H) (specific activity 100 Ci mmol^{-1}, Biotrend) using the microcentrifuge method (Kirchman et al., 1985; Smith and Azam, 1992). Duplicate samples and one killed control (1.5 mL each) were labeled using ^{3}H-leucine at a final concentration of 20 nmol L^{-1}. BP was determined down to 800 m depth and, for practical reasons, we chose an incubation temperature of 14 °C as an average over this depth interval. However, in this paper, only data from the top 100 m depth are shown and BP rates were corrected for the difference between incubation and *in situ* temperature (Eq. 4). All samples were incubated for 6 h in the dark with headspace. Controls were poisoned with trichloroacetic acid. All Samples were measured on board with a liquid scintillation analyzer (Packard Tri-Carb, model 1900 A). ^{3}H-leucine uptake was converted to carbon units by applying a conversion factor of 1.55 kg C mol^{-1} leucine (Simon and Azam, 1989).

BP rates from incubations at 14 °C were converted to BP rates at 22 °C following the equation from López-Urrutia and Morán (2007):

$$BP_{22°C} = BP_{14°C} \times 1.906 \quad (Eq. 4)$$

Community respiration rates (CR) were estimated from quadruplicate incubations by measuring changes of dissolved oxygen over 24-36 hours at the same temperature as used for BP (14 °C) using optode spot mini sensors (PreSens PSt3; Precision Sensing GmbH, Regensburg, Germany). The detection limit (DL) for CR was 0.55 µmol O$_2$ L^{-1} d^{-1}.

CR at 22°C was estimated using the extrapolation from Regaudie-De-Gioux and Duarte (2012):

$$CR_{22°C} = CR_{14°C} \times 2.011 - 0.013 \quad (Eq. 5)$$

CR$_{22°C}$ was converted into bacterial respiration (BR$_{22°C}$) after Aranguren-Gassis et al. (2012):

$$BR_{22°C} = 0.30 \times CR_{22°C}^{1.22} - 0.013 \quad (Eq. 6)$$

A respiratory quotient of 1 was used to convert oxygen consumption into carbon respiration (del Giorgio and Cole 1998).

We estimated the bacterial carbon demand (BCD) as follows:

$$BCD = BP + BR \quad (Eq. 7)$$

Bacterial growth efficiency (BGE) was calculated from BP and BCD:

$$BGE = \frac{BP}{BCD} \quad \text{(Eq. 8)}$$

Detailed information on procedures and calculations of microbial activities are provided in the SI.

2.4 Data analysis

Statistical analyses and calculations were conducted using the software R (v4.0.3) in R studio (v1.1.414; Ihaka and Gentleman 1996). Analysis of variances (ANOVA) and Tukey test, were performed on the different parameters by grouping the station by their position (SI Table **S1**). Seawater density was calculated using R package oce v1.3.0 (Kelley, 2018) and the mixed layer maximum depth was determined as the depth at which a change from the surface density of 0.125 kg m^{-3} has occurred (Levitus, 1982). Other R packages used in this study include corrplot v0.84 (Dray, 2008) and ggplot2 v3.3.3 (Wickham, 2016). Section plots were made using Ocean Data View v5.6.2 (Schlitzer, 2020). Depth integrated values were calculated using the midpoint rule.

3. Results

3.1 Hydrographic conditions

Along the zonal transect, open ocean waters (from 20 to 24.5 °W) had a temperature range of 13.45-24.2 °C and a salinity between 35.55-36.79 in the upper 200 m depth (Fig. **2a** and **b**). The average mixed layer depth was 30 ± 2 m (Fig. **3a**; SI Table **S1**). Oxygen concentrations (Fig. **2c**) decreased with depth while nutrient concentrations increased (Fig. **2d-e**). Nutrients were depleted (<0.5, <0.2, and <0.5 µmol L^{-1} for DIN, PO$_4$, Si(OH)$_4$, respectively) in the mixed layer.

At the coastal stations (16.51 to 16.92 °W), the temperature had a range of 14.6-26.1 °C and a salinity between 35.53 and 36.08 in the upper 200 m depth (Fig. **2a** and **b**). Here, the mixed layer was significantly shallower than in the open ocean (Tukey, $p<0.01$), with an average depth of 17 ± 4 m (Fig. **3a**; SI Table **S1**). Oxygen was decreasing with depth and a shallow oxygen minimum zone (OMZ; <50 µmol kg^{-1}) was detected between 80 m and 200 m depth (Fig. **2c**). Nutrients (Fig. **2d-e**) were depleted at the surface (5 m depth), while the deeper coastal waters (~ 80 to 200 m depth) were colder and richer in nutrients than the open ocean waters, with on average 3.4-fold higher nutrient concentrations (DIN, PO4, Si(OH)$_4$) when integrated over 100 m depth (data not shown).

333 In the CE ('periphery' and 'core'), waters had a temperature range of 13.2-24.2 °C and a salinity

334 between 35.48 and 36.36 in the upper 200 m depth (Fig. **2a** and **b**). A compression of isopycnals

335 with a strong doming of the isotherms, isohalines, and nutriclines was observed (Fig. **2a-b**, **d-**

336 **f**). A shallow OMZ was detected from ~30 m to ~100 m depth with the lowest oxygen

337 concentration (<10 µmol kg^{-1}) between 30-40 m. The mixed layer was significantly shallower

338 (Tukey, $p<0.05$) in the CE periphery than in all other stations, with an average of 15 ± 6 m

339 depth (Fig. **3a**). However, the CE core was not significantly different from the open ocean (20

340 ± 2 m; Tukey, $p>0.05$). At the surface (5 m depth), nutrients were depleted (<0.5, <0.2 and <0.5

341 µmol L^{-1} for DIN, PO$_4$, Si(OH)$_4$, respectively) only in the most eastern (17.11 °W, 18 °N) and

342 western (18.83-19.11 °W, 18.58 °N) part of the CE periphery **(**Fig. **2d-f**). In the core, nutrient

343 concentrations were also lowest in the surface water, but richer in nutrients than in the ambient

344 waters.

345 The Frontal Zone station E3 (19.55 °W) was distinct from the adjacent stations with respect to

346 surface temperature (1 °C colder, Fig **2a**). A doming of the nutriclines was observed **(**Fig.**2d-f**)

347 and nutrient concentrations integrated over 100 m depth at St. E3 were ~3 fold higher than at

348 the open ocean S4 (20.3 °W) and ~1.2 fold higher than at the CE periphery St. EDZ-1 (19.11

349 °W).
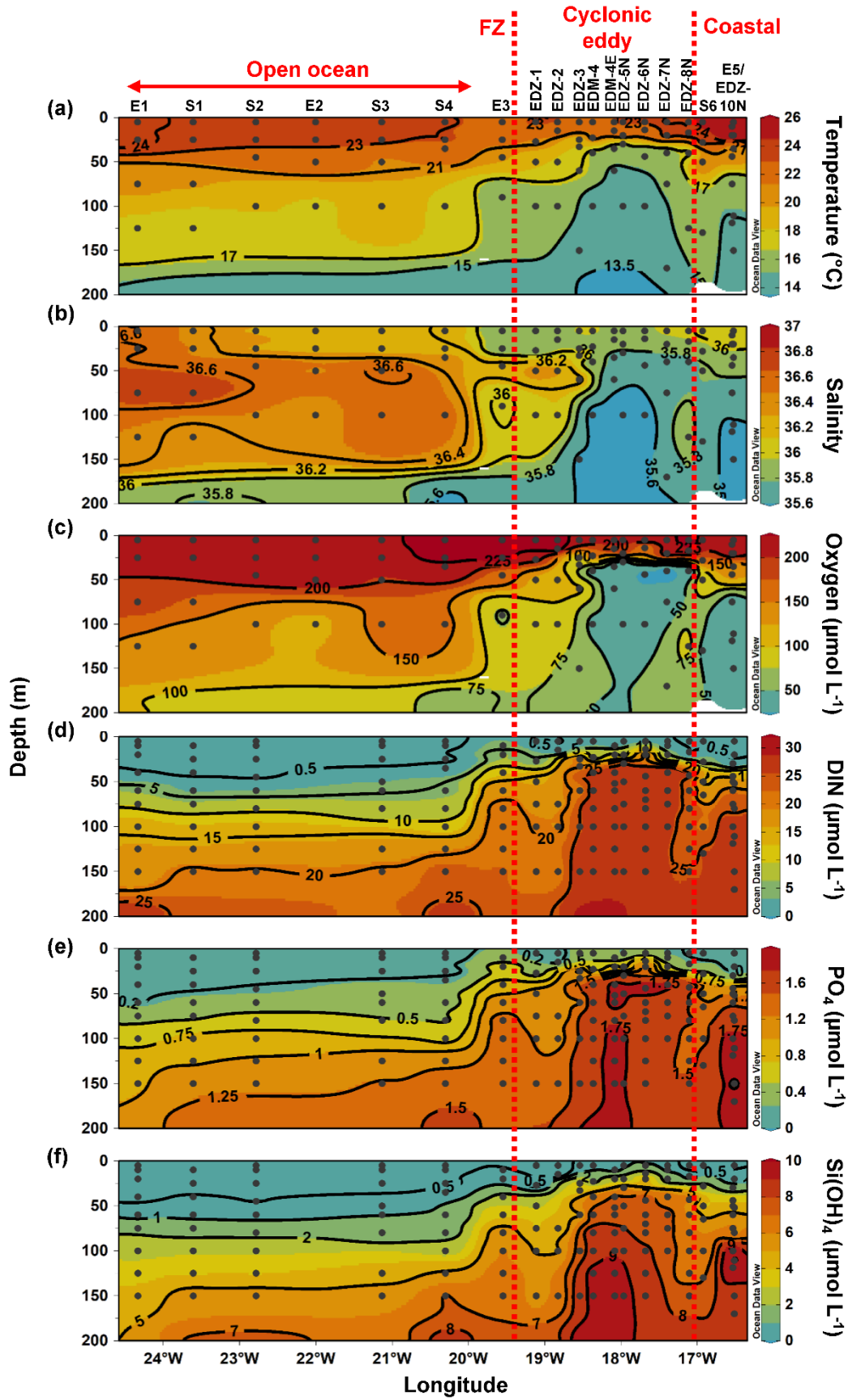
Figure 2: Epipelagic distribution (0-200 m) of temperature (**a**), salinity (**b**), oxygen (**c**), total inorganic nitrogen (DIN) (**d**), phosphate (PO_4) (**e**), and silicate ($Si(OH)_4$, (**f**). Red dashed lines show the western and eastern boundary of the cyclonic eddy periphery, respectively. FZ refers to Frontal Zone.

3.2 Chlorophyll-*a* and primary production

In order to compare stations along the zonal transect and within the eddy, data were integrated over the water column (0-100 m depth). Along the zonal transect, depth-integrated Chl-*a* concentration ranged between 11.7 and 58.7 mg m^{-2} and decreased from the coastal to the open ocean stations (Table **1**; Fig. **3b**). Depth-distribution showed a Chl-*a* maximum in the open ocean around ~75 m from 23.61 to 24.33 °W and around ~50 m from 22.78 to 20.3 °W, up to 0.68 µg L^{-1} (Fig. **4a**). At the coastal stations, the Chl-*a* maximum was found between 30-40 m depth with values up to 0.96 µg L^{-1}. Integrated biomass of autotrophic pico-and nanoplankton (Table **1**) ranged between 1.6 and 7.8 and between 3.6 and 6.1 g C m^{-2} in the open ocean and at the coastal stations, respectively. In the open ocean waters, the depth distribution of autotrophic pico-and nanoplankton biomass (Fig. **4b**) showed a gradient from west to east with a concentration maximum at ~75 m from 23.61 to 24.33 °W, a concentrations maximum at ~50 m from 22 to 22.78 °W, and a concentrations maximum between 5-25 m from 21.13 to 20.3 °W. Concentrations reached up to 166 µg C L^{-1}. At the coastal stations, the maximum autotrophic pico-and nanoplankton biomass was found between 30-40 m depth with values up to 117 µg C L^{-1}. Both Chl-*a* concentration and autotrophic pico-and nanoplankton biomass did not vary significantly between the open ocean and the coastal stations (Tukey, $p>0.05$). Integrated total and dissolved primary production (PP$_{TOT}$; PP$_{DOC}$; Table **1**) remained fairly constant with ranges of 101-137 and 42.8-78 mmol C m^{-2} d^{-1}, respectively, at the coastal and the open ocean stations. An exception was the station furthest offshore (24.33 °W), where rates decreased sharply to 25.8 mmol C m^{-2} d^{-1} for PP$_{TOT}$ and to 12.3 mmol C m^{-2} d^{-1} for PP$_{DOC}$. The integrated percentage of extracellular release (PER; Table **1**) ranged between 42.3 and 67.5%. PP$_{DOC}$ and PER did not vary significantly between the open ocean and the coastal stations (Tukey, $p>0.05$). PP$_{TOT}$ and PP$_{DOC}$ decreased with depth except for station E2 (Fig. **4c**), while PER increased (Fig. **4d**).
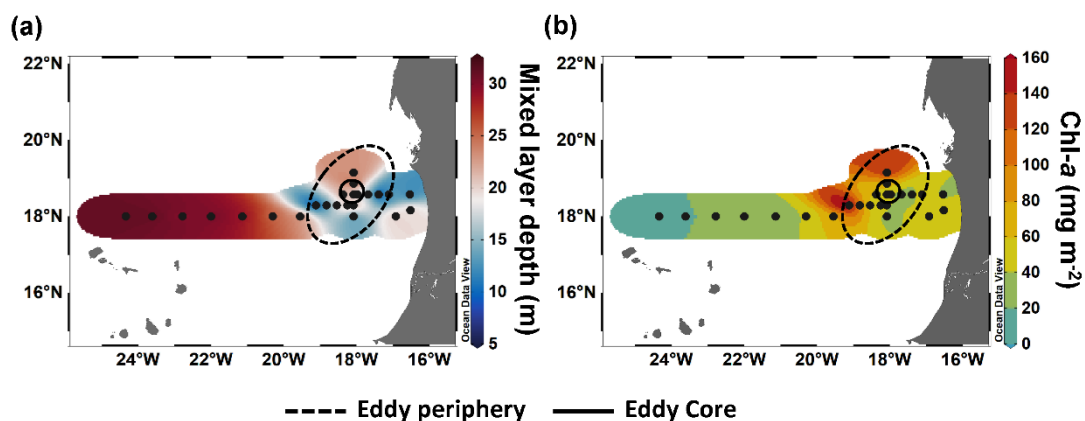
Figure 3: Spatial distribution of maximum mixed layer depth (**a**) and integrated chlorophyll *a* (Chl-*a*) over 100 m depth (**b**) during M156.

In the CE (core and periphery) and at the Frontal Zone, integrated Chl-*a* concentration ranged from 17.2 to 225 mg m^{-2} (Table **1**). The Chl-*a* distribution (Fig. **3a**) showed a clear spatial separation with the highest values (98.7-225 mg m^{-2}) in the western and northern (148 mg m^{-2}) parts of the CE and lowest values (26.8-37.5 mg m^{-2}) in the southern and eastern part. Depth distribution of Chl-*a* concentration also differed across the eddy, with values >0.5 µg L^{-1} reaching down to 45 m depth at the Frontal Zone and the western part of the CE and down to 30 m depth in the eastern part of the CE (Fig. **4a**). Highest concentrations were detected in the western part of the eddy with 8.7 µg L^{-1} at station EDZ-1 at 27 m. Within the upper 30 m, Chl-*a* concentration within the CE was significantly higher than at the open ocean and the coastal stations (ANOVA, *p*<0.05). Integrated autotrophic pico-and nanoplankton biomass ranged between 0.3 and 4.7 g C m^{-2} in the CE (Table **1**). Depth distribution of autotrophic pico-nanoplankton biomass (Fig. **4b**) showed low biomass in the upper 40 m (<25 µg C L^{-1}) from 18.83 to 19.11 °W. In contrast, higher biomass (>25 µg C L^{-1}) occurred in the more eastern stations of the CE (17.11 to 18.54 °W) and westwards from the Frontal Zone (19.55 °W). In the eddy, autotrophic pico- and nanoplankton biomass reached higher concentrations mainly within the upper 40 m, with values up to 191 µg C L^{-1}. Depth-integrated PP$_{TOT}$ and PP$_{DOC}$ rates were significantly higher in the CE and at the Frontal Zone than in the open ocean and the coastal stations (Tukey, *p*<0.05) with values ranging from 245 to 687 mmol C m^{-2} d^{-1} and from 95.9 to 238 mmol C m^{-2} d^{-1}, respectively (Table **1**). PP$_{TOT}$ rates (Fig. **4c**; Table **2**) were fairly constant across the CE's surface (5 m depth), ranging between 11.2 and 13.7 µmol C L^{-1} d^{-1}, but varied strongly between 15-40 m depth (0.2-14.5 µmol C L^{-1} d^{-1}). The highest PP$_{TOT}$ rates were found in the Frontal Zone with up to 25.0 µmol C L^{-1} d^{-1} at the surface. The range of PP$_{DOC}$ rates (Table **2**; Fig. **4d**) was larger in the CE (0.2-4.9 µmol C L^{-1} d^{-1}) and the Frontal Zone (0.7-7.8 µmol C L^{-1} d^{-1}) than in the open ocean and at the coastal stations. Integrated PER had a range of 29.4-40.8 % (Table **1**). Compared to open ocean and coastal stations, a slightly lower PER was observed within the upper 40 m (Fig. **4e**) for the CE and Frontal Zone.

Table 1: Chlorophyll *a* (Chl-*a*) and abundance, biomass and activity of phyto- and bacterial plankton, integrated over the upper 100 m depth. '-' indicate that the variable was not measured. Sampling date, time and depth can be found in SI Table **S1**.

Location	Station	Chl-*a* (mg m^{-2})	Autpico-nanoPl (g C m^{-2})	PP$_{DOC}$ (mmol C m^{-2} d^{-1})	PP$_{TOT}$ (mmol C m^{-2} d^{-1})	PER (%)	HB (10^{15} cell m^{-2})	CR (mmol C m^{-2} d^{-1})	BR (mmol C m^{-2} d^{-1})	BP (mmol C m^{-2} d^{-1})
Coastal	E5	54.5	6.1	75.2	137	54.9	14.7	99.6	32	5.6
	EDZ-10N	36.8	3.6	-	-	-	13.8	-	-	7.9
	AZM-3	58.7	5.3	-	-	-	12.9	-	-	10.8
Eddy Periphery	EDZ-8N	61.5	4.7	-	-	-	10.7	-	-	15.6
	EDZ-7N	26.8	1.6	-	-	-	9.4	-	-	10.8
	EDZ-6N	27.9	1.2	-	-	-	9.1	-	-	7.5
Eddy Core	EDZ-5N	39.2	4.1	-	-	-	14.5	154	59.1	9.0
	EDM-4E	46.0	3.3	95.9	245	39.2	15.2	135	60.8	8.6
	EDM-3E	77.5	3.2	-	-	-	15.3	-	-	16.4
	EDM-4	63.8	3.3	141	380	37.2	19.4	275	127	12.2
Eddy Periphery	EDM-6E	35.7	3.6	117	288	40.8	23.7	-	-	13.0
	EDM-5E	35.2	1.6	-	-	-	11.8	-	-	9.0
	EDM-2E	148	1.7	-	-	-	20.8	-	-	21.8
	EDZ-4	47.8	1.0	-	-	-	14.4	-	-	12.0
	EDZ-3	17.2	0.3	-	-	-	9.6	-	-	5.6
	EDZ-2	98.7	0.7	131	445	29.4	8.2	592	320	15.5
	EDZ-1	225	0.6	-	-	-	13.7	-	-	36.7
Frontal Zone	E3	72.1	2.4	238	687	34.6	12.9	529	257	14.7
Open ocean	S4	40.2	4.5	-	-	-	16.9	-	-	8.2
	S3	30.7	4.0	42.8	101	42.3	14.5	346	148	5.0
	E2	22.3	4.4	78.0	116	67.5	12.2	387	168	3.9
	S2	34.1	7.8	-	-	-	13.9	-	-	4.4
	S1	12.2	1.6	-	-	-	5.4	-	-	1.4
	E1	11.7	2.3	12.3	25.8	47.6	6.7	19.7	6.3	1.6
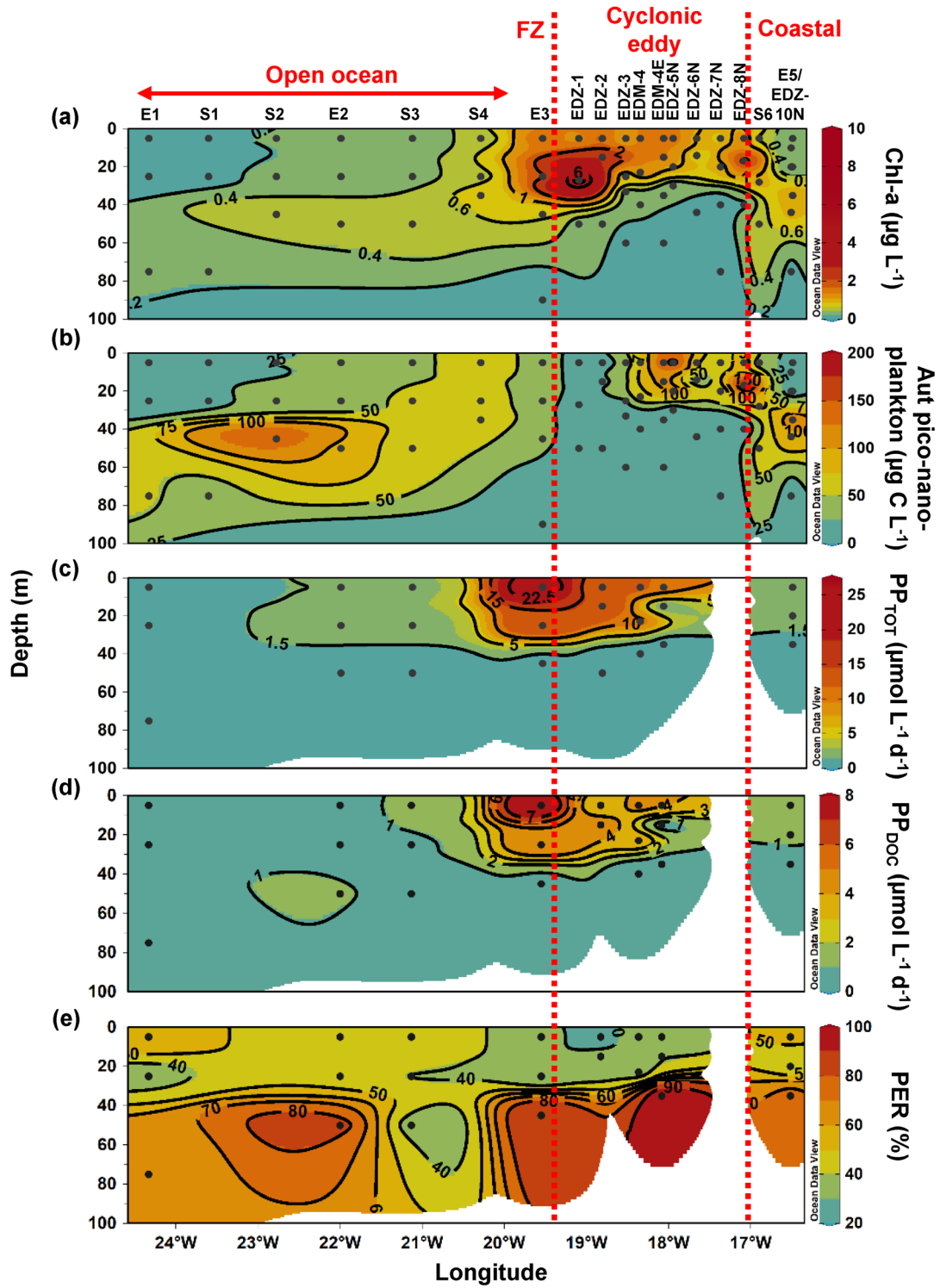
Figure 4: Depth distribution of phytoplankton biomass and activity from the surface to 100 m. Chlorophyll *a* (Chl-*a;* **a**), Autotrophic pico-and nanoplankton biomass (Aut pico-nanoplankton; **b**), total primary production (PP$_{TOT}$; **c**), dissolved primary production (PP$_{DOC}$; **d**) and percentage of extracellular release (PER; **e**). Red dashed lines show the western and eastern boundary of the cyclonic eddy periphery, respectively. FZ refers to Frontal Zone.

3.3 Bacterial abundance and activities

Heterotrophic bacterial abundance decreased with depth and was highest in the upper 50 m at all stations (Fig. **5a**). At the coastal and open ocean stations, integrated (0-100 m) heterotrophic bacteria abundance ranged between 12.9-14.7 and $5.4\text{-}16.9 \times 10^{15}$ cells m^{-2}, respectively (Table **1**). No significant differences in heterotrophic bacterial abundance were observed between the open ocean and coastal stations (Tukey, $p > 0.05$). In the open ocean waters, the lowest integrated BR and CR rates were observed at the station furthest offshore (E1), with 6.3 and 19.7 mmol C m^{-2} d^{-1}, respectively (Table 1). At the other open ocean stations, integrated BR and CR rates ranged between 148-168 mmol C m^{-2} d^{-1} and 346-348 mmol C m^{-2} d^{-1}, respectively, which was higher than at the coastal station with BR rates of 32 mmol C m^{-2} d^{-1} and CR rates of 98 mmol C m^{-2} d^{-1}. Overall, BR and CR rates were higher in the open ocean stations than in the coastal ones with highest rates (> 1 and > 2.5 µmol C L^{-1} d^{-1}, respectively) in the top 60 m (Fig. **5b**; SI Fig. **S4a**). Integrated BP, in contrast, was generally higher at the coastal stations with 5.6-10.8 mmol C m^{-2} d^{-1} compared to the open ocean ones with 1.4-8.2 mmol C m^{-2} d^{-1} (Table **1**). However, volumetric BP rates were not significantly different from the open ocean (Tukey $p > 0.05$), where BP rates were more variable. At the coastal stations, the highest BP rates were observed either at the surface (5 m) or at around ~40 m depth, while in the open ocean, the highest rates were constantly found in the surface samples (Fig. **5c**). BGE was determined for the upper 50 m and showed little variability with depth (Table **2**; Fig. **5d**). However, BGE was significantly higher (Tukey, $p < 0.05$) at the coastal stations ($9.6 \pm 3.7\%$ to $14.1 \pm 1.7\%$) compared to the open ocean ones (1.7 ± 0.1 to $4.2 \pm 0.04\%$). We estimated the predominance of autotrophy/heterotrophy in the system, by dividing the PP$_{TOT}$ rates by CR (Mouriño-Carballido and McGillicuddy 2006). Heterotrophic conditions ($\frac{PP_{TOT}}{CR} < 1$) occurred at the open ocean stations throughout the water column, while autotrophic conditions ($\frac{PP_{TOT}}{CR} > 1$) prevailed at the coastal St. E5 ($\frac{PP_{TOT}}{CR}$ ratio ranging from 0.7 to 1.9; Table **2**). This pattern was preserved when data were integrated over the mixed layer (Fig. **6**). PP$_{DOC}$ rates were sufficient to satisfy the BCD at the coastal St. E5, but not in the open ocean stations (Table **2**).

In the CE and at the Frontal Zone, integrated heterotrophic bacterial abundance ranged from $8.2\text{-}23.7 \times 10^{15}$ cells m^{-2} (Table **1**). In the CE, substantial variation of bacterial abundance occurred within the upper 20 m (Fig. **5a**), with an abundance of $< 1 \times 10^9$ cells L^{-1} in the western periphery of the CE and $> 3 \times 10^9$ cells L^{-1} in the CE core stations. Depth-integrated BR and CR ranged between 59.1 and 320 and between 135 and 592 mmol C m^{-2} d^{-1}, respectively (Table **1**).

457   Elevated BR and CR rates (> 1 and 2.5 μmol C L^{-1} d^{-1}, respectively) were only present in the

458   upper ~30-40 m of the CE (Fig. **5b**; SI Fig. **S4a**). Integrated BP rates ranged from 5.6 to 36.7

459   mmol C m^{-2} d^{-1} in the CE and at the Frontal Zone stations (Table **1**). BP rates were elevated in

460   the upper 40 m of the CE and at the Frontal Zone, and significantly higher than in the majority

461   of the coastal and open ocean stations (Tukey *p*<0.05). Stations in the core of the CE had BGEs

462   (Table **2**; Fig. **5d**) significantly higher than at the stations located in the open ocean (Tukey,

463   *p*<0.05). BGE had a range of 2.7 ± 2.9 to 18.3 ± 1.0 % and 5.1 ± 0.2 to 5.5 ± 2.4% in the CE

464   and the Frontal Zone stations, respectively. Highest BGE was observed at 15 m depth in the CE

465   core (18.3%, St. EDM-4E). The CE and Frontal Zone stations showed net hetero- as well as net

466   autotrophy (Table **2**), with a $\frac{PP_{TOT}}{CR}$ ratio ranging from 0.2 to 1.9. When integrated over the mixed

467   layer (Fig. **6**), stations within the core of the CE and at the Frontal Zone were net autotrophic,

468   with a $\frac{PP_{TOT}}{CR}$ ratio ranging from 1.42 to 1.85, while net heterotrophy occurred at the eddy

469   periphery. PP$_{DOC}$ was on average equivalent to 71% of the BCD within the CE and at the Frontal

470   Zone, ranging from 27.9 to 110% (Table **2**).
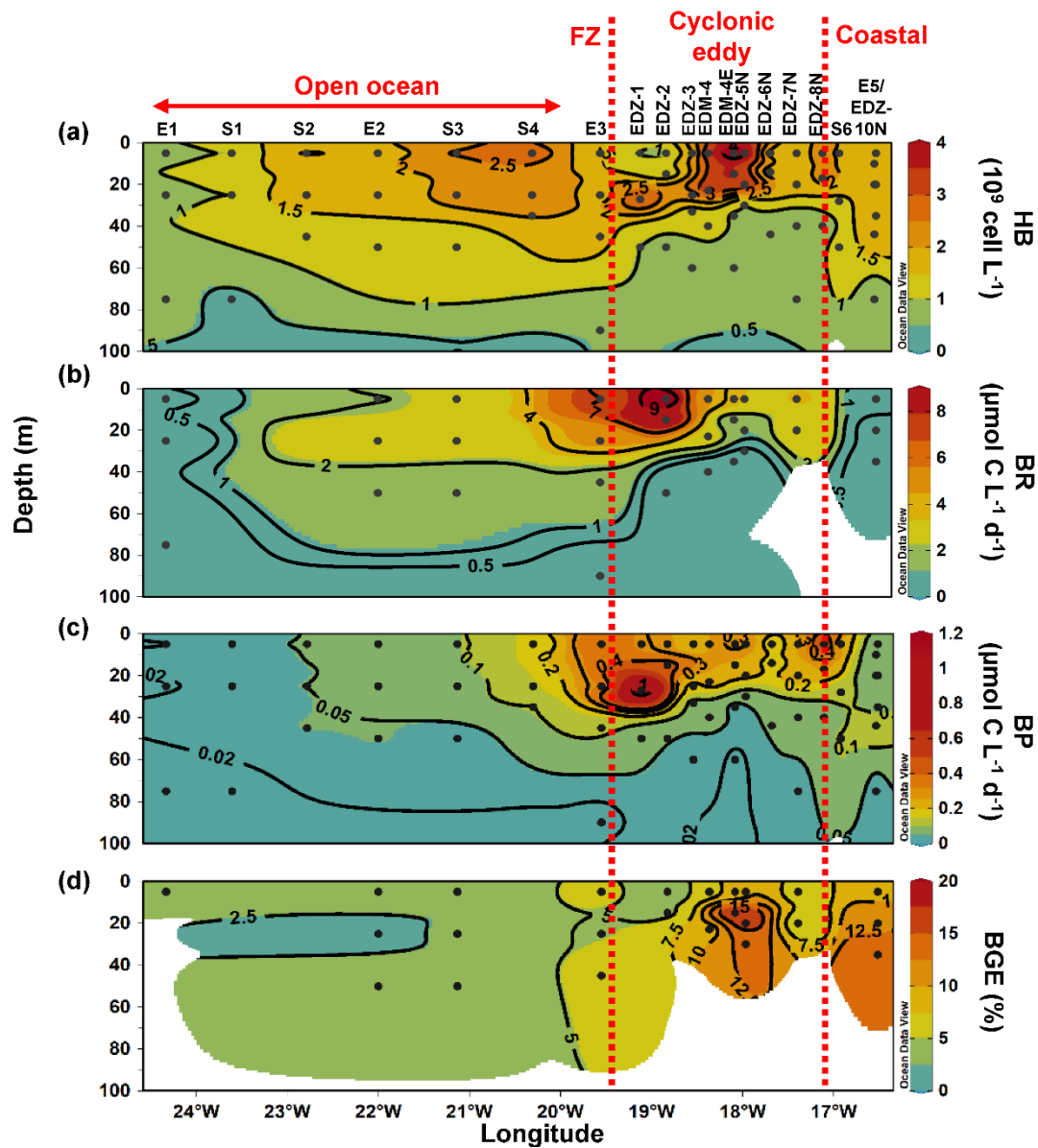
Figure 5: Depth distribution of heterotrophic bacterial abundance and activities from the surface to 100 m. Heterotrophic bacterial abundance (HB; **a**), bacterial respiration (BR; **b**), bacterial production (BP; **c**), bacterial growth efficiency (BGE; **d**). Red dashed lines show the western and eastern boundary of the cyclonic eddy periphery, respectively. FZ refers to Frontal Zone. BP and CR rates at *in-situ* temperature were estimated based on López-Urrutia and Morán (2007) and on Regaudie-de-Gioux and Duarte (2012). BR rates were estimated from measured and temperature-corrected CR rates based on Aranguren-Gassis et al, (2012). Details are provided in the methods section and the SI.

480 Table 2: Average (mean) ± standard deviation of microbial metabolic activities during M156: bacterial
481 carbon demand (BCD); bacterial growth efficiency (BGE); dissolved primary production (PP_{DOC});
482 Percentage of extracellular release (PER); total primary production (PP_{TOT}), the ratio between PP_{DOC}
483 and BCD ($\frac{PP_{DOC}}{BCD}$) and the ratio between PP_{TOT} and CR ($\frac{PP_{TOT}}{CR}$). BCD and BGE were obtained from
484 temperature-corrected BP and BR rates (see text). '-' indicate that the parameter was not measured and
485 'B.D.' below detection (see text). Sampling date, time and depth are given in SI Table **S1**.

Location	Station	Depth (m)	BCD (μmol C L^{-1} d^{-1})	BGE (%)	CR (μmol C L^{-1} d^{-1})	PP_{DOC} (μmol C L^{-1} d^{-1})	PER (%)	PP_{TOT} (μmol C L^{-1} d^{-1})	$\frac{PP_{DOC}}{BCD}$ (%)	$\frac{PP_{TOT}}{CR}$
Coastal	E5	5	0.6 ± 0.1	9.6 ± 3.7	1.7 ± 0.5	1.5 ± 0.2	34.9 ± 1.1	2.7 ± 0.2	217.4	1.6 ± 0.4
		20	0.5 ± 0.1	12.2 ± 2.6	1.3 ± 0.4	1.2 ± 0.1	52.6 ± 2.7	2.5 ± 0.1	231.4	1.9 ± 0.4
		35	0.5 ± 0.3	14.1 ± 1.7	1.3 ± 0.9	0.7 ± 0.1	89.8 ± 3.9	1.0 ± 0.1	143.2	0.7 ± 0.1
	EDZ-10N	All	-	-		-	-	-		-
	S6	All	-	-		-	-	-		-
Eddy Periphery	EDZ-8N	All	-	-		-	-	-		-
	EDZ-7N	5	3.6 ± 0.8	6.6 ± 0.5	7.3 ± 1.9	-	-	-		-
		20	3.6 ± 0.3	6.2 ± 2.6	7.3 ± 0.9	-	-	-		-
	EDZ-6N	All	-	-		-	-	-		-
Eddy Core	EDZ-5N	5	2.8 ± 0.4	10.9 ± 2.5	5,6 ± 1.1	-	-	-		-
		20	1.2 ± 0.4	16.7 ± 3.7	2.8 ± 1.1	-	-	-		-
		30	0.4 ± 0.6	12.7 ± 0.5	1.2 ± 1.7	-	-	-		-
		100	B.D.	B.D.		-	-	-		-
	EDM-4E	5	4.7 ± 0.5	7.5 ± 1.9	8.9 ± 1.3	4.3 ± 0.1	36.7 ± 0.2	11.2 ± 0.1	87.9	1.3 ± 0.1
		15	1.4 ± 0.4	18.3 ± 1.0	3.1 ± 1.3	0.4 ± 0.1	39.3 ± 6.8	1.1 ± 0.1	29.5	0.3 ± 0.1
		35	B.D.	B.D.		0.6 ± 0.3	94.4 ± 0.9	0.6 ± 0.3		-
		60	B.D.	B.D.		-	-	-		-
	EDM-3E	All	-	-		-	-	-		-
	EDM-4	5	4.8 ± 1.1	5.9 ± 2.7	9,3 ± 2.9	4.3 ± 1.0	35.1 ± 5.7	12.6 ± 1.2	92.3	1.4 ± 0.4
		23	3.6 ± 0.2	8.1 ± 3.5	7.1 ± 0.7	3.9 ± 0.2	35.7 ± 1.4	11.0 ± 0.3	110.0	1.5 ± 0.4
		40	B.D.	B.D.		0.3 ± 0.1	85.3 ± 7.1	0.3 ± 0.1		-
		100	B.D.	B.D.		-	-	-		-
Eddy Periphery	EDM-6E	5	-	-		4.8 ± 0.4	34.9 ± 1.1	13.7 ± 0.7		-
		25	-	-		3.4 ± 0.3	52.6 ± 2.7	6.5 ± 0.4		-
		32	-	-		0.2 ± 0.1	89.8 ± 3.9	0.2 ± 0.1		-
	EDM-5E	All	-	-		-	-	-		-
	EDM-2E	All	-	-		-	-	-		-
	EDZ-4	All	-	-		-	-	-		-
	EDZ-3	All	-	-		-	-	-		-

486

487 Table 2 continued:

Location	Station	Depth (m)	BCD (μmol C L^{-1} d^{-1})	BGE (%)	CR (μmol C L^{-1} d^{-1})	PP$_{DOC}$ (μmol C L^{-1} d^{-1})	PER (%)	PP$_{TOT}$ (μmol C L^{-1} d^{-1})	$\frac{PP_{DOC}}{BCD}$ (%)	$\frac{PP_{TOT}}{CR}$
Eddy Periphery	EDZ-2	5	10.6 ± 0.7	2.7 ± 2.9	18.2 ± 1.4	2.9 ± 0.3	25.1 ± 3.4	11.9 ± 1.0	27.9	0.7 ± 0.7
		15	9.6 ± 2.5	4.6 ± 1.3	16.5 ± 5.3	4.9 ± 0.1	31.0 ± 1.7	14.5 ± 0.6	46.8	0.9 ± 0.1
		50	B.D.	B.D.		0	-	-0		-
		100	B.D.	B.D.		-	-	-		-
	EDZ-1	All	-	-		-	-	-		-
Frontal Zone	E3	5	7.3 ± 0.5	5.5 ± 2.4	13.1 ± 1.3	7.8 ± 0.4	31.7 ± 1.7	25.0 ± 0.9	108.1	1.9 ± 0.7
		25	5.0 ± 1.2	5.1 ± 0.2	9.5 ± 2.9	5.0 ± 0.6	33.4 ± 3.2	14.3 ± 0.8	96.3	1.5 ± 0.3
		45	1.9 ± 0.7	5.4 ± 4.0	4.4 ± 1.8	0.7 ± 0.2	87.0 ± 3.3	0.8 ± 0.2	37.8	0.2 ± 0.1
		90	B.D.	B.D.		-	-	-		-
Open ocean	S4	All	-	-		-	-	-		-
	S3	5	3.2 ± 0.6	3.0 ± 0.4	6.9 ± 1.6	1.3 ± 0.2	49.1 ± 5.5	2.7 ± 0.3	41.4	0.4 ± 0.2
		25	2.6 ± 0.5	3.1 ± 2.1	5.7 ± 1.5	1.16 ± 0.03	38.4 ± 0.9	2.5 ± 0.03	36.8	0.4 ± 0.1
		50	1.2 ± 1.1	3.3 ± 0.3	3.0 ± 2.9	0.0 ± 0.01	21.8 ± 6.6	0.1 ± 0.01	2.6	0.0 ± 0.01
		100	B.D.	B.D.		-	-	-		-
	E2	5	1.8 ± 0.6	3.4 ± 0.4	4.3 ± 1.7	0.6 ± 0.1	40.9 ± 3.4	1.38 ± 0.1	31.4	0.3 ± 0.1
		25	3.5 ± 1.1	1.7 ± 0.1	7.4 ± 2.9	0.94 ± 0.1	50.2 ± 3.1	1.89 ± 0.1	27.1	0.3 ± 0.1
		50	1.7 ± 0.4	2.9 ± 0.8	4.2 ± 1.2	1.25 ± 0.3	91.3 ± 2.5	1.4 ± 0.3	72.6	0.3 ± 0.3
		100	B.D.	B.D.		-	-	-		-
	S2	All	-	-		-	-	-		-
	S1	All	-	-		-	-	-		-
	E1	5	0.4 ± 0.3	4.2 ± 0.04	1.3 ± 0.9	0.23 ± 0.1	54.7 ± 13.3	0.39 ± 0.1	52.4	0.3 ± 0.1
		25	B.D.	B.D.		0.18 ± 0.01	38.5 ± 0.6	0.43 ± 0.01		-
		75	B.D.	B.D.		0.08 ± 0.02	61.7 ± 6.2	0.13 ± 0.02		-
		125	B.D.	B.D.		-	-	-		-

488

489

3.5 Semi-labile dissolved organic carbon

Between coastal and open ocean stations, SL-DOC concentration was not significantly different (Tukey, $p>0.05$; SI Fig. **S4b**) with ranges of 1.9-8.0 µmol L^{-1} at the coastal and 1.6-18.9 µmol L^{-1} at the open ocean stations. At those sites, SL-DOC distribution was rather uniform in the upper 40 m with SL-DOC > 5 µmol L^{-1}, except from the station furthest offshore (St. E1) where SL-DOC > 5 µmol L^{-1} was limited to shallow depths (5 m). In the CE and at the Frontal Zone, SL-DOC concentration was clearly elevated and increased from east to west with an overall range of 1.4-54.4 µmol L^{-1}. At the Frontal Zone, SL-DOC concentration > 5 µmol L^{-1} was detectable down to 90 m depth.
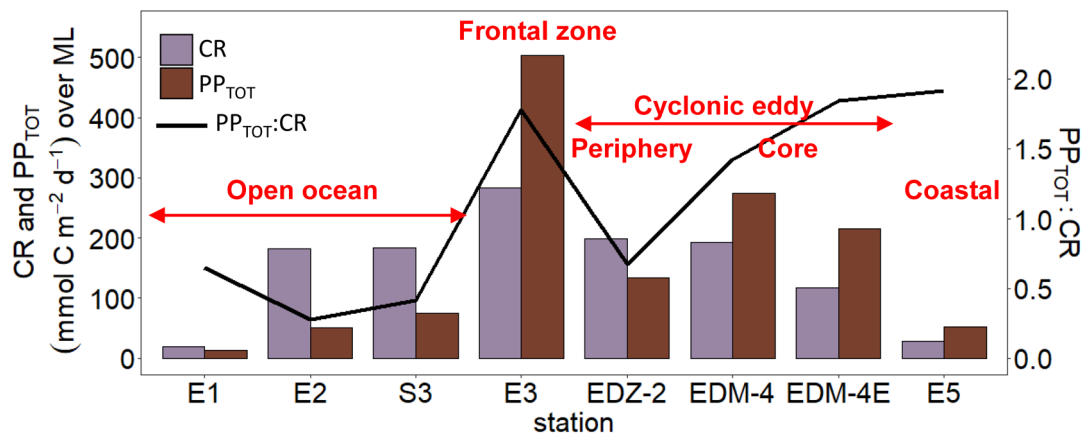
Figure 6: Integrated total primary production (PP_{TOT}) and community respiration (CR) rates over the mixed layer during M156.

3.6 Correlation analysis

We applied a Pearson correlation matrix (Fig. **7**) to reveal significant correlations between the measured parameters in the stations outside (open ocean + coastal) and inside (cyclonic eddy + frontal zone) the area influenced by the eddy. In both regimes, temperature correlated negatively with nutrients (DIN, PO_4, $Si(OH)_4$; r =-0.70, -0.67 and -0.67 respectively for the stations outside and r = -0.97, -0.96 and -0.95 for the stations inside the area influenced by the eddy, $p<0.001$) and positively with bacterial abundances (r = 0.51 and 0.68 respectively, $p<0.001$).

In the stations outside the influence of the eddy, total (PP_{TOT}) and dissolved primary production (PP_{DOC}) rates were not correlated to Chl-*a* or autotrophic pico-and nanoplankton biomass, $p>0.05$). In contrast, heterotrophic bacterial abundance (HB) and the bacterial biomass

production (BP) were correlated to primary productivity rates ($r = 0.85$ and $r = 0.82$ respectively for PP_{TOT} and r= 0.77 and 0.77 respectively for PP_{DOC}, $p<0.001$), Chl-*a* ($r=0.64$ and 0.72 respectively, $p<0.001$) and autotrophic pico-and nanoplankton biomass, ($r=0.42$ and 0.46 respectively, $p<0.001$) and the concentration of semi-labile DOC (SL-DOC; $r = 0.61$ and 0.56 , $p<0.001$). However, bacterial respiration (BR), was not correlated to any variable ($p>0.05$).

In the stations influenced by the eddy, PP_{TOT} was positively correlated to Chl-*a* ($r= 0.55$, $p<0.05$) whereas PP_{DOC} ($r=0.47$, $p>0.05$) was not, and both were not correlated to the autotrophic pico- and nanoplankton biomass. Chl-*a* and SL-DOC were significantly correlated ($r=0.36$, p<0.001). Heterotrophic bacterial and autotrophic pico- and nanoplankton abundance and activities were coupled but differently than in the stations outside the eddy. HB was not correlated to PP_{TOT} and PP_{DOC} ($p>0.05$), but was strongly correlated to Chl-*a* and autotrophic pico-and nanoplankton biomass ($r=0.57$ and 0.76, respectively, $p<0.001$) but not to SL-DOC ($r=0.19$, $p>0.05$). BP, on the contrary, was correlated to PP_{TOT} and PP_{DOC} ($r=0.63$ and 0.59, respectively, $p<0.05$) and strongly to Chl-*a* ($r=0.92$, $p<0.001$). BP correlated also to autotrophic pico-and nanoplankton biomass and to SL-DOC, albeit to a lesser extent ($r=0.41$ and 0.43, respectively, $p<0.05$). In contrast to stations not influenced by the eddy, BR was strongly correlated to Chl-*a* and SL-DOC ($r=0.83$ and 0.76, respectively, $p<0.001$). However, BR was not significantly correlated to autotrophic pico-and nanoplankton biomass, $PP_{TOT,}$ and PP_{DOC} ($r= -0.05$, 0.61 and 0.50 respectively, $p>0.05$).
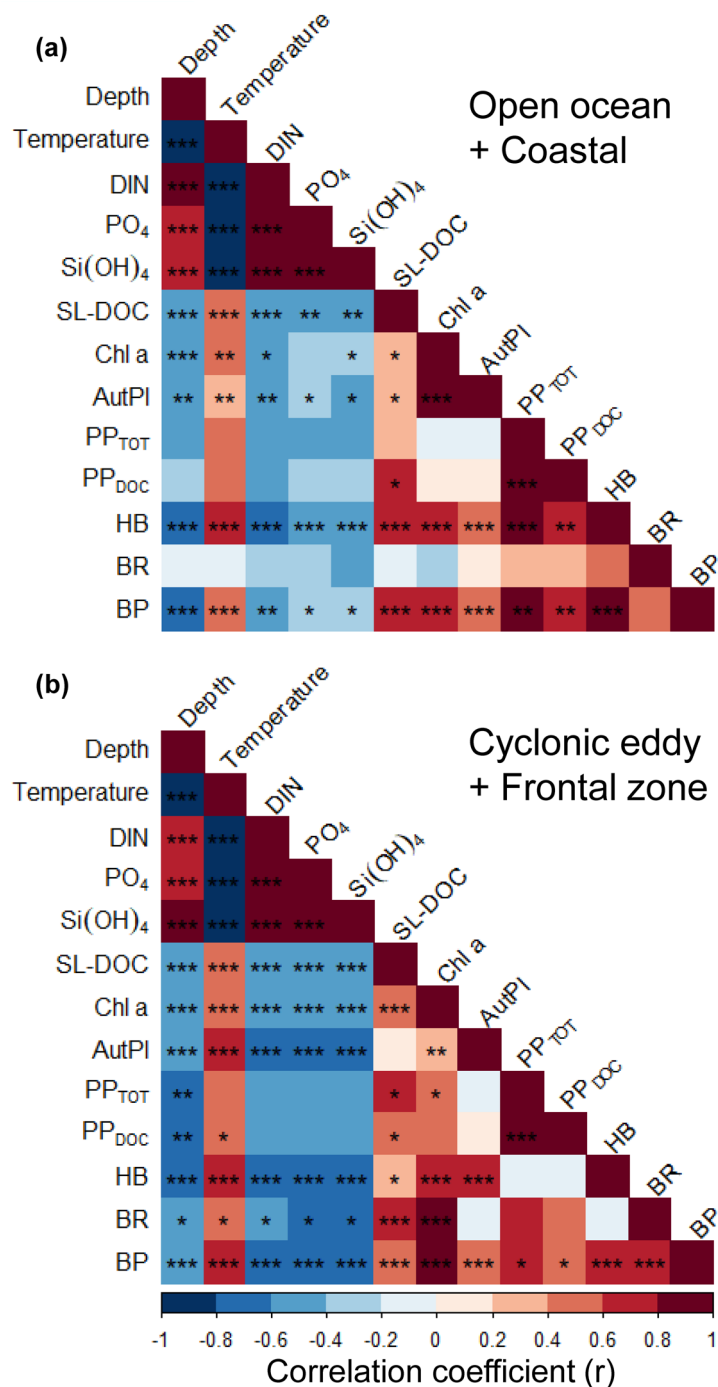
Figure 7: Pearson correlation matrix of biochemical parameters, metabolic activities, and bacterial abundance in the upper 100 m in samples not influenced by the cyclonic eddy (i.e., coastal and open ocean stations) (a) and samples influenced by the cyclonic eddy (b). Statistical significance: '***'< 0.001, '**'< 0.01, '*'< 0.05.

4. Discussion

4.1 Effect of a cyclonic eddy on the distribution of phytoplankton abundance and activity in the Mauritanian upwelling system

In general, coastal Chl-*a* concentration during this study was not as high as observed in earlier studies with strong coastal upwelling (e.g., Alonso-Sáez et al., 2007; Agustí and Duarte, 2013; Arístegui et al., 2020). This might be related to the relatively weak upwelling resulting from weak surface winds along the Mauritanian Coast typically occurring during summer when our samples were collected (Pelegrí and Peña-Izquierdo, 2015). Consequently, during summer, fewer nutrients reach the euphotic zone. At the same time, offshore surface wind remained strong, enhanced vertical mixing and may explain why coastal Chl-*a* concentration was only slightly higher compared to the open ocean. When excluding the eddy-influenced stations, there was no marked gradient in phytoplankton productivity either, unlike other regions of the CanUS (Demarcq and Somoue, 2015; Arístegui et al., 2020). PP_{TOT} and PP_{DOC} rates stayed rather constant from the coast to the open ocean and were in the range of reported rates in oligotrophic offshore waters of the CanUS (Agustí and Duarte, 2013; Lasternas et al., 2014). Spatial distribution of SL-DOC was relatively uniform as well when considering the coastal and open ocean stations only. PER in our study was on average $51.1 \pm 17\%$ in both the open ocean and the coastal stations, which contrasts previous findings. For example, Agustí and Duarte (2013) reported PER to range from ~1% in 'healthy' communities from the upwelled waters of the CanUS to ~70% in 'dying' communities from the oligotrophic waters of the ETNA. PER have been reported to increase with nutrient depletion (Obernosterer and Herndl, 1995; Agustí and Duarte, 2013; Lasternas et al., 2014; Piontek et al., 2019) among other factors (see review by Mühlenbruch et al., 2018). Since upwelling was weak during our sampling period, low nutrient concentrations in the surface waters might explain the relatively high PER that we observed near the coast.

The CE broke this rather uniform distribution of phytoplankton productivity from the coastal to the open ocean waters. Chl-*a* isolines were pushed towards the surface in the CE (Fig. **4a**). Similar uplifting of Chl-*a* isolines towards the surface has been reported for other eddies (Lochte and Pfannkuche, 1987; Feng et al., 2007; Noyon et al., 2019) and might result from phytoplankton relocation through intense vertical mixing by strong surface winds (Feng et al., 2007; Noyon et al., 2019). Before our eddy survey, strong surface winds occurred offshore (SI Fig. **S5**), which might explain the high Chl-*a* concentration (>0.5 µg L^{-1}) that we found at the surface (5 m) of all stations within the CE. Within the eddy, we observed that Chl-*a* was higher in the western than in the eastern part of the eddy (Fig. **3b** and **4a**). Chelton et al. (2011) showed

based on satellite observation that due to the rotational flow and the westward propagation of CEs, Chl-*a* tends to accumulate in their southwest quadrants while being lower in their northeast quadrants. To the best of our knowledge, this is the first time that high-resolution in situ sampling could demonstrate this specific submesoscale Chl-*a* distribution within a CE. Outside of the CE boundaries, we noticed a thermal front with colder surface water. Thermal fronts have been detected outside of the periphery of eddies and interpreted to result from eddy-eddy interaction (See review by Mahadevan, 2016) and/or eddy-wind interaction (Xu et al., 2019). In this Frontal Zone, we observed higher nutrient concentrations than in the adjacent stations including the western part of the CE periphery and a doming of the nutriclines, which indicates upwelling (see Fig. **2**). Consequently, Chl-*a* was elevated, and 'compressed' to the surface in this area similarly as in the CE (Fig. **4a**).

Our flow cytometry data (SI Fig. **S6**) showed that cyanobacteria (*Synechococcus*) and eukaryotic pico- and nanoplankton within the CE were unevenly distributed. This suggests that the phytoplankton community of the CE was likely distinct from the surrounding waters, but also variable on the submesoscale within the CE. This is consistent with previous studies on phytoplankton distributions in eddies (e.g., Lochte and Pfannkuche, 1987; Lasternas et al., 2013; Hernández-Hernández et al., 2020). Moreover, the mixed layer was also highly variable within the CE and so were PP_{TOT} rates (SI Table **S1**, Figs. **3** and **6**). We observed a three-fold variation of depth-integrated PP_{TOT} rates over 100m depth (Table **1**) within the CE which is coherent with earlier observations of a five-fold variation of primary production integrated over the euphotic zone in a CE in the subtropical Pacific Ocean (Falkowski et al., 1991). Overall, primary productivity was enhanced within the CE and the Frontal Zone with an average of four-fold more depth-integrated PP_{TOT} rates over 100 m depth than in the open ocean and coastal stations. This is coherent with Löscher et al. (2015), who found that depth-integrated primary productivity over the Chl-*a* maximum of a CE in the Mauritanian upwelling system was three-fold higher than in the surrounding waters. Exracellular release rates (PP_{DOC}) were also enhanced within the eddy, but PER was slightly lower at the eddy surface (Fig. **4d**, **e**). We emit two hypotheses regarding this distribution: 1) the lower PER was due to a higher proportion of larger phytoplankton (e.g., diatoms), which have lower turnover rates and therefore lower PER and/or 2) the upwelling of nutrients generated by the CE might have enhanced the physiological health of the phytoplankton community.

4.2 Variations in heterotrophic bacterial abundance and activity associated with a cyclonic eddy

Along the zonal transect, in the stations not affected by the eddy (open ocean+coastal stations), a significant positive correlation was observed between HB abundance and PP_{TOT} rates (Fig. **7a**). Those variables were rather uniformly distributed from the coast to the offshore waters excluding samples influenced by the eddy, which is in agreement with earlier findings by Bachmann et al. (2018) for the Mauritanian upwelling system during summer. Both our BR and BP were also within the range of reported rates for coastal and offshore waters of the CanUS (Reinthaler et al., 2006; Alonso-Saez et al., 2007; Vaqué et al., 2014). BP rates slightly decreased from the coast to the open ocean when samples from the eddy were not considered. Similar trends were found in the CanUS with different upwelling intensities and during different seasons (Alonso-Saez et al., 2007; Vaqué et al., 2014). The distinct distribution of BP and BR rates affected the distribution of the BGE, which was higher in the coastal than in the open ocean stations. Overall, our BGEs represent the lower end of global ocean values, but similarly low BGEs have been observed for other EBUS, such as the CanUS (Alonso-Sáez et al., 2007) the California upwelling system (del Giorgio et al., 2011) and the Humboldt upwelling system (Maßmig et al., 2020). Yet, we report an average BGE two times lower than Alonso-Sáez et al. (2007), which may be due to differences in upwelling intensity. Indeed, Kim et al. (2017) denoted that BGE increased with increasing upwelling intensity in the Ulleung Basin. At the coast, PP_{DOC} rates were sufficient to compensate for the BCD, indicating a strong trophic dependence of bacteria on phytoplankton, whereas in the open ocean PP_{DOC} rates covered up between 2.6 to 78% indicating a much lower trophic dependence of bacteria on phytoplankton. Therefore, in the open ocean, other carbon sources (i.e., PP_{POC}, SL-DOC) must have been used to compensate the BCD. SL-DOC compounds have a turnover of weeks to months, which allows them to escape rapid microbial degradation (Hansell et al., 2009). Consequently, we hypothesize that the BCD in the open ocean was sustained through SL-DOC produced in excess near the coast and transported offshore. Indeed, in the CanUS, currents and eddies have been shown to laterally transport DOC offshore up to 2000 km (Lovecchio et al., 2018).

Within the CE-influenced stations (CE + Frontal Zone), HB abundance was disconnected from the PP_{TOT} rates (Fig. **7b**). For example, in the southwestern periphery and the frontal zone HB abundanceds were relatively low, while both PP_{TOT} rates and Chl-*a* concentrations were relatively high (Fig. **4a**, **c**). Hernández-Hernández et al. (2020) reported a similar observation with a strong heterogeneity of HB biomass distribution within a CE in the CanUS. Attachment

to particles, viral lysis or grazing by nanoflagellates might have led to a selective reduction in HB abundance. However, the exact reasons for the low HB occurrence at the eddy periphery and the Frontal Zone are unknown. Despite the low HB abundance, BP was particularly stimulated in these areas. On average, BP was three-fold higher in the eddy influenced stations compared to the open ocean ones when integrated over 100 m. This is in accordance with earlier studies from the Sargasso Sea (Ewart et al., 2008), the CanUS (Baltar et al., 2010), and the Mediterranean Sea (Belkin et al., 2022), where enhanced BP has been observed in CE. As stated previously, the upwelling induced by the CE and the Frontal Zone led to higher phytoplankton biomass, which was likely responsible for this overall increase in BP. However, it is noteworthy that BP and PP_{TOT} rates were less correlated than in the zonal transect. BR rates were also enhanced at the surface of the CE and followed a similar trend as BP. SL-DOC concentrations showed a strong positive correlation with BR, which makes sense considering that high molecular weight DOC compounds (>1 kDa) are a favourable carbon source for heterotrophic microbes (Amon and Benner, 1994, 1996; Benner and Amon, 2015). PP_{DOC} rates in the CE covered 27.9% to 110% of the BCD, indicating a moderate to strong trophic dependence of bacteria on phytoplankton in CE. Although PP_{TOT} globally may satisfy the BCD in the CE (43.1-341%) a question remains about why BGE was low in the CE (2.7-18.3%).

Overall, we showed that autotrophy prevails in the upper 100 m depth of Mauritanian coastal waters while heterotrophy prevailed offshore. This is coherent with a modeling study from Lovecchio et al. (2017). The CE and the associated Frontal Zone fuelled phytoplankton nutrient needs and maintained autotrophy further offshore inside of the eddy and especially in the Frontal Zone, where highest PP_{TOT} were measured. Mouriño-Carballido (2009) reported from indirect estimations of net community production that the frontal zones between CEs and ACEs are among the most productive areas in the North-West subtropical Atlantic Ocean. Previous studies have shown that the trophic balance could switch from autotrophy to heterotrophy in an eddy within a month (Maixandeau et al., 2005; Mouriño-Carballido and McGillicuddy, 2006). Here we showed that both autotrophy and heterotrophy can occur within a single eddy. This urges the need for more high-resolution eddy studies in order to better estimate their impact on plankton metabolic activities and carbon cycling.

Conclusion

Our results highlight the ability of a CE to be an autotrophic vector toward the open ocean with organic matter freshly produced by the phytoplankton community inside. Yet, despite the strong

autotrophy associated with the CE, phytoplankton exudation of DOM was not always enough to compensate for bacterial metabolic needs. Even if BP was enhanced in the CE, the BGE was rather low and varied substantially. Instead, heterotrophic bacteria preferentially used DOM for respiration. Microbial metabolic activity dynamics within eddies are complex and require further investigations to better understand and unravel carbon cycling in these features.

Data availability

All data will be made available at the PANGEA database (data manager, webmaster: Hela Mehrtens)

Author contribution

QD, KWB and AE designed the scientific study, analyzed the data and wrote the paper. AB, did the eddy reconstruction and both AB and JH commented on the paper.

Competing interests:

The authors declare that they have no conflict of interest.

Acknowledgments

We thank the captain and the crew of the *R/V Meteor* for their support during the M156 cruise. We thank J. Roa, T. Klüver and L. Scheidemann for sampling on board. We thank J. Roa and S. Golde additionally for the analysis of dissolved organic matter and T. Klüver for cell counting, bacterial and phytoplankton activities analyses. We thank B. Domeyer and R. Suhrberg for the nutrient analyses. This study has been conducted using E.U. Copernicus Marine Service Information. The results contain modified Copernicus Climate Change Service information 2020. Neither the European Commission nor ECMWF is responsible for any use that may be made of the Copernicus information or data it contains. This study is a contribution

of the REEBUS project (Role of Eddies in the Carbon Pump of Eastern Boundary Upwelling Systems) sub-projects WP1 and WP4, funded by the BMBF (funding reference no. 03F0815A).

Reference

Agustí, S., and Duarte, C. M.: Phytoplankton lysis predicts dissolved organic carbon release in marine plankton communities, Biogeosciences, 10, 1259-1264, https://doi.org/10.5194/bg-10-1259-2013, 2013.

Alonso-Sáez, L., Gasol, J. M., Arístegui, J., Vilas, J. C., Vaqué, D., Duarte, C. M., and Agustí, S.: Large-scale variability in surface bacterial carbon demand and growth efficiency in the subtropical northeast Atlantic Ocean, Limnol. Oceanogr., 52, 533-546, https://doi.org/10.4319/lo.2007.52.2.0533, 2007.

Amon, R. M. W., and Benner, R.: Rapid cycling of high molecular weight dissolved organic matter in the ocean, Nature 369, 549–552. doi: 10.1038/369549a0, 1994.

Anderson, T. R., and Ducklow, H. W.: Microbial loop carbon cycling in ocean environments studied using a simple steady-state model, Aquat. Microb. Ecol., 26, 37-49. 2001.

Aranguren-Gassis, M., Teira, E., Serret, P., Martínez-García, S., and Fernández, E.: Potential overestimation of bacterial respiration rates in oligotrophic plankton communities, Mar. Ecol. Prog. Ser., 453, 1–10, https://doi.org/10.3354/meps09707, 2012.

Arístegui, J., Barton, E. D., Álvarez-Salgado, X. A., Santos, A. M. P., Figueiras, F. G., Kifani, S., Hernández-León, S., Mason, E., Machú, E., and Demarcq, H.: Sub-regional ecosystem variability in the Canary Current upwelling, Prog. Oceanogr., 83, 33-48, https://doi.org/10.1016/j.pocean.2009.07.031, 2009.

Arístegui, J., Montero, M. F., Hernández-Hernández, N., Alonso-González, I. J., Baltar, F., Calleja, M. L., and Duarte, C. M.: Variability in Water-Column Respiration and Its Dependence on Organic Carbon Sources in the Canary Current Upwelling Region, Front. Earth Sci., 8, 1-12. https://doi.org/10.3389/feart.2020.00349/, 2020.

Arístegui, J., Tett, P., Hernández-Guerra, A., Basterretxea, G., Mon- tero, M. F., Wild, K., Sangrá, P., Hernández-León, S., Cantón, M., García-Braun, J. A., Pacheco, M., and Barton,

E. D.: The influence of island-generated eddies on Chl a distribution: a study of mesoscale variation around Gran Canaria, Deep-Sea Res., 44:71-96. 1997.

Arnon, R. M. W., and Benner, R: Bacterial utilization of different size classes of dissolved organic matter. Limnol. Oceanogr., 41(l), 41–51, 1996.

Bachmann, J., Hassenrück, C., Gärdes, A., Iversen, M. H., Heimbach, T., Kopprio, G. A., and Grossart, H. P.: Environmental Drivers of Free-Living vs. Particle-Attached Bacterial Community Composition in the Mauritania Upwelling System. Front. Microbiol., 9, 1–13, https://doi.org/10.3389/fmicb.2018.02836, 2018.

Baltar, F., Arístegui, J., Gasol, J. M., Lekunberri, I., and Herndl, G. J.: Mesoscale eddies: Hotspots of prokaryotic activity and differential community structure in the ocean. ISME J., 4, 975-988, https://doi.org/10.1038/ismej.2010.33, 2010.

Belkin, N., Guy-haim, T., Rubin-blum, M., Lazar, A., and Sisma-, G.: Influence of cyclonic and anti-cyclonic eddies on plankton biomass , activity and diversity in the southeastern Mediterranean Sea. Ocean Sci., 18, 693–715, https://doi.org/10.5194/os-18-693-2022, 1–56, 2022.

Benner, R., and Amon, R. M. W.: The size-reactivity continuum of major bioelements in the ocean. Annu. Rev. Mar. Sci. 7, 185–205. doi: 10.1146/annurev-marine-010213-135126, (2015).

Borchard, C. and Engel, A.: Organic matter exudation by Emiliania huxleyi under simulated future ocean conditions, Biogeosciences, 9, 3405–3423, doi:10.5194/bg-9-3405-2012, 2012

Carlson, C. A.: Production and Removal Processes. Chapter 4 in Biogeochemistry of Marine Dissolved Organic Matter, Editor(s): Hansell D. A., Carlson, C. A. AP, 805, 91–151. https://doi.org/10.1016/b978-012323841-2/50006-3. 2002.

Chelton, D. B., Gaube, P., Schlax, M. G., Early, J. J., and Samelson, R. M.: The Influence of Nonlinear Mesoscale Eddies on Near-Surface Oceanic Chlorophyll. Science 334, 328–333, 2011.

Cheney, R. E., and Richardson, P. L.: Observed Decay of a Cyclonic Gulf Stream Ring, Deep-Sea Res. Oceanogr. Abstr., 23, 143-155, https://doi.org/10.1016/S0011-7471(76)80023-X, 1976.

Cherrier, J., Valentine, S. K., Hamill, B., Jeffrey, W. H., and Marra, J. F.: Light-mediated release of dissolved organic carbon by phytoplankton. J. Mar. Syst., 147: 45–51, 2015.

Christaki, U., Gueneugues, A., Liu, Y., Blain, S., Catala, P., Colombet, J., Debeljak, P., Jardillier, L., Irion, S., Planchon, F., Sassenhagen, I., Sime-Ngando, T., & Obernosterer, I.: Seasonal microbial food web dynamics in contrasting Southern Ocean productivity regimes. Limnol. Oceanogr., 66(1), 108–122, https://doi.org/10.1002/lno.11591, 2021.

Couespel, D., Lévy, M., andand Bopp, L.: Oceanic primary production decline halved in eddy-resolving simulations of global warming, Biogeosciences, 18(14), 4321-4349, https://doi.org/10.5194/bg-18-4321-2021, 2021.

D'Asaro, E. A.: Generation of submesoscale vortices: A new mechanism, J. Geophys. Res., 93, 6685-6693, https://doi.org/10.1029/JC093iC06p06685, 1988.

del Giorgio, P. A., and Cole, J. J.: Bacterial Growth Efficiency in Natural Aquatic Systems. Annu. Rev. Ecol. Evol. Syst., 29, 503-541, https://doi.org/10.1146/annurev.ecolsys.29.1.503, 1998.

Del Giorgio, P. A., Condon, R., Bouvier, T., Longnecker, K., Bouvier, C., Sherr, E., and Gasol, J. M.: Coherent patterns in bacterial growth, growth efficiency, and leucine metabolism along a northeastern Pacific inshore – offshore transect. Limnol. Oceanogr., 56(1), 1–16, https://doi.org/10.4319/lo.2011.56.1.0001, 2011.

Demarcq, H. and Somoue, L.: Phytoplankton and primary productivity off Northwest Africa. In: Oceanographic and biological features in the Canary Current Large Marine Ecosystem. Valdés, L. and Déniz-González, I. (eds). IOC-UNESCO, Paris. IOC Technical Series, No. 115, pp. 161-174. URI: http://hdl.handle.net/1834/9186.2015.

Descy, J. P., Leporcq, B., Viroux, L., François, C., and Servais, P.: Phytoplankton production, exudation and bacterial reassimilation in the River Meuse (Belgium). J. Plankton Res., 24(3), 161-166. https://doi.org/10.1093/plankt/24.3.161, 2002.

Dickson, A. G., Sabine, C. L., and Christian, J. R.: Guide to Best Practices for Ocean CO2 measurements. PICES Special Publication 3, 191 pp., 2007.

Dittmar, T., Cherrier, J., and Ludwichowski, K. U.: The analysis of amino acids in seawater, in: Practical guidelines for the analysis of seawater, ed. by Oliver Wurl Boca Raton [u.a.], CRC Press, ISBN: 978-1-4200-7306-5, 2009.

Dray, S.: On the number of principal components: A test of dimensionality based on measurements of similarity between matrices, Comput. Stat. Data Anal., 52, 4, 2228-2237, 2008.

Engel, A., Borchard, C., Piontek, J., Schulz, K. G., Riebesell, U., and Bellerby, R.: CO_2 increases 14C primary production in an Arctic plankton community. Biogeosciences, 10(3), 1291–1308. https://doi.org/10.5194/bg-10-1291-2013, 2013.

Engel, A., Händel, N., Wohlers, J., Lunau, M., Grossart, H. P., Sommer, U., and Riebesell, U.: Effects of sea surface warming on the production and composition of dissolved organic matter during phytoplankton blooms: Results from a mesocosm study, J. Plankton Res., 33(3), 357-372, https://doi.org/10.1093/plankt/fbq122, 2011.

Engel, A., Thoms, S., Riabesell, U., Rochelle-Newall, E., and Zondervan, I.: Polysaccharide aggregation as a potential sink of marine dissolved organic carbon. Nature, 428(6986), 929–932. https://doi.org/10.1038/nature02453, 2004.

Evans, C. A., O'Reily, J. E., and Thomas, J. P.: A handbook for measurement of Chl a a and primary production, College Station, TX: Texas A andM University, 1987.

Ewart, C. S., Meyers, M. K., Wallner, E. R., McGillicuddy, D. J., and Carlson, C. A.: Microbial dynamics in cyclonic and anticyclonic mode-water eddies in the northwestern Sargasso Sea, Deep-Sea Res. II: Top. Stud. Oceanogr., 55(10-13), 1334-1347. https://doi.org/10.1016/j.dsr2.2008.02.013, 2008.

Falkowski, P. G., Ziemann, D., Kolber, Z., and Bienfang P. K.: Role of eddy pumping in enhancing primary production in the ocean, Letters to Nature, Vol 352, 1991.

Feng, M., Majewski, L. J., Fandry, C. B., and Waite, A. M.: Characteristics of two counter-rotating eddies in the Leeuwin Current system off the Western Australian coast, Deep-Sea Res. II: Top. Stud. Oceanogr., 54(8-10), 961-980, https://doi.org/10.1016/j.dsr2.2006.11.022, 2007.

Gargas, E.: A Manual for Phytoplankton Primary Production Studies in the Baltic, The Baltic Marine Biologists, 2, 88 p., 1975.

Gasol, J.M., del Giorgio, P.A.,: Using flow cytometry for counting natural planktonic bacteria and understanding the structure of planktonic bacterial communities. Sci. Mar. 64, 197–224. 2000.

819   Gattuso J. P., Epitalon J. M., Lavigne H. and Orr J.,: seacarb: seawater carbonate chemistry,
820   R package version 3.2.13, http://CRAN.R-project.org/package=seacarb, 2020.

821   Grasshoff K., Kremling K., Ehrhardt M. : Methods of sea- water analysis. Wiley-VCH,
822   Weinheim, 1999.

823   Hansell, D. A., Carlson, C. A., Repeta, D. J., and Schlitzer, R.: Dissolved organic matter in
824   the ocean a controversy stimulates new insights. Oceanogr., 22(SPL.ISS. 4), 202–211.
825   https://doi.org/10.5670/oceanog.2009.109, 2009.

826   Hernández-Hernández, N., Arístegui, J., Montero, M. F., Velasco-Senovilla, E., Baltar, F.,
827   Marrero-Díaz, Á., Martínez-Marrero, A., and Rodríguez-Santana, Á.: Drivers of Plankton
828   Distribution Across Mesoscale Eddies at Submesoscale Range, Front. Mar. Sci., 7, 1-13.
829   https://doi.org/10.3389/fmars.2020.00667, 2020.

830   Ihaka R., and Gentleman R.: R: a language for data analysis and graphics. J. Comput. Graph.
831   Stat. 5, 299, 1996

832   Jiao, N., Robinson, C., Azam, F., Thomas, H., Baltar, F., Dang, H., Hardman-Mountford,
833   N. J., Johnson, M., Kirchman, D. L., Koch, B. P., Legendre, L., Li, C., Liu, J., Luo, T., Luo,
834   Y. W., Mitra, A., Romanou, A., Tang, K., Wang, X., Zhang, R. Mechanisms of microbial
835   carbon sequestration in the ocean - Future research directions. Biogeosciences, 11(19),
836   5285–5306. https://doi.org/10.5194/bg-11-5285-2014. 2014.

837   Karstensen, J., Fiedler, B., Schütte, F., Brandt, P., Körtzinger, A., Fischer, G., Zantopp, R.,
838   Hahn, J., Visbeck, M., and Wallace, D.: Open ocean dead zones in the tropical North
839   Atlantic Ocean, Biogeosciences, 12, 2597-2605, https://doi.org/10.5194/bg-12-2597-2015,
840   2015.

841   Kelley, D. E.: Oceanographic Analysis with R. Oceanographic Analysis with R.
842   https://doi.org/10.1007/978-1-4939-8844-0, 2018.

843   Kim, B., Kim, S. H., Kwak, J. H., Kang, C. K., Lee, S. H., and Hyun, J. H.: Heterotrophic
844   bacterial production, respiration, and growth efficiency associated with upwelling intensity
845   in the Ulleung Basin, East Sea. Deep Sea Res. Part II Top. Stud. Oceanogr., 143, 24-35,
846   https://doi.org/10.1016/j.dsr2.2017.07.002, 2017.

Kirchman, D., K'nees, E., and Hodson, R.: Leucine incorporation and its potential as a measure of protein synthesis by bacteria in natural aquatic systems, Appl. Environ. Microbiol., 49(3), 599-607, https://doi.org/10.1128/aem.49.3.599-607.1985, 1985.

Lasternas, S., and Agustí, S.: The percentage of living bacterial cells related to organic carbon release from senescent oceanic phytoplankton, Biogeosciences, 11, 6377-6387, https://doi.org/10.5194/bg-11-6377-2014, 2014.

Lasternas, S., Piedeleu, M., Sangrà, P., Duarte, C. M., and Agustí, S.: Forcing of dissolved organic carbon release by phytoplankton by anticyclonic mesoscale eddies in the subtropical NE Atlantic Ocean. Biogeosciences, 10(3), 2129-2143, https://doi.org/10.5194/bg-10-2129-2013, 2013.

Lathuilière, C., Echevin, V., and Lévy, M.: Seasonal and intraseasonal surface Chl a-a variability along the northwest African Coast, J. Geophys. Res. Oceans, 113, C05007. https://doi.org/10.1029/2007JC004433, 2008.

Le Vu, B., Stegner, A., Arsouze, T.: Angular momentum eddy detection and tracking algorithm (AMEDA) and its application to coastal eddy formation, J. Atmos. Oceanic Technol. 35, 739-762. https://doi.org/10.1175/JTECH-D-17-0010.1, 2018.

Levitus, S.: Climatological atlas of the World Ocean. NOAA Prof. Pap. 13, 1–41, 1982.

Lévy, M., Klein, P., and Treguier, A. M.: Impact of submesoscale physics on production and subduction of phytoplankton in an oligotrophic regime, J. Mar. Res., 59(4), 535-565, 2001.

Lindroth P., Mopper K.: High performance liquid chromatographic determination of subpicomole amounts of amino acids by precolumn fluorescence derivatization with o-phthaldialdehyde, Anal. Chem., 51, 1667-1674, https://doi:10.1021/ac50047a019, 1979.

Lipson, D. A.: The complex relationship between microbial growth rate and yield and its implications for ecosystem processes. Front. Microbiol., 1–5. https://doi.org/10.3389/fmicb.2015.00615. 2015.

Lochte, K., and Pfannkuche, O.: Cyclonic cold-core eddy in the eastern North Atlantic. II. Nutrients, phytoplankton and bacterioplankton, Mar. Ecol. Prog. Ser., 39, 153-164. https://doi.org/10.3354/meps039153, 1987.

Lønborg, C., Martínez-García, S., Teira, E., and Álvarez-Salgado, X. A.: Bacterial carbon demand and growth efficiency in a coastal upwelling system. Aquat. Microb. Ecol., 63(2), 183–191. https://doi.org/10.3354/ame01495, 2011.

López-Urrutia, Á., and Morán, X. A. G.: Resource limitation of bacterial production distorts the temperature dependence of oceanic carbon cycling, Ecology, 88(4), 817-822, https://doi.org/10.1890/06-1641, 2007.

Löscher, C. R., Fischer, M. A., Neulinger, S. C., Fiedler, B., Philippi, M., Schütte, F., Singh, A., Hauss, H., Karstensen, J., Körtzinger, A., Künzel, S., and Schmitz, R. A.: Hidden biosphere in an oxygen-deficient Atlantic open-ocean eddy: Future implications of ocean deoxygenation on primary production in the eastern tropical North Atlantic, Biogeosciences, 12, 7467-7482, https://doi.org/10.5194/bg-12-7467-2015, 2015.

Lovecchio, E., Gruber, N., and Münnich, M: Mesoscale contribution to the long-range offshore transport of organic carbon from the Canary Upwelling System to the open North Atlantic. Biogeosciences, 15(16), 5061–5091. https://doi.org/10.5194/bg-15-5061-2018, 2018.

Lovecchio, E., Gruber, N., Münnich, M., and Lachkar, Z.: On the long-range offshore transport of organic carbon from the Canary Upwelling System to the open North Atlantic, Biogeosciences, 14(13), https://doi.org/10.5194/bg-14-3337-2017, 2017.

Mahadevan, A.: The Impact of Submesoscale Physics on Primary Productivity of Plankton, Annu. Rev. Mar. Sci., 8, 161-184, https://doi.org/10.1146/annurev-marine-010814-015912, 2016.

Maixandeau, A., Lefevre, D., Karayanni, H., Christaki, U., VanWambeke, F., Thyssen, M., Denis, M., Fernandez, C.I., Uitz, J., Leblanc, K., Queguiner, B.: Microbial community production, respiration, and structure of the microbial food web of an ecosystem in the northeastern Atlantic Ocean, J. Geophys. Res. Oceans, 110 (C7), C07S17, 2005.

Maßmig, M., Lüdke, J., Krahmann, G., and Engel, A:. Bacterial degradation activity in the eastern tropical South Pacific oxygen minimum zone. Biogeosciences, 17(1), 215–230. https://doi.org/10.5194/bg-17-215-2020, 2020.

McGillicuddy Jr, D. J., Anderson, L. A., Doney S. C., and Maltrud, M. E.: Eddy-driven sources and sinks of nutrients in the upper ocean: Results from a 0 . 1 ° resolution model of

the North Atlantic, Glob. Biogeochem. Cycles., 17(2), 1035, https://doi.org/10.1029/2002GB001987, 2003.

McGillicuddy, D. J.: Mechanisms of Physical-Biological-Biogeochemical Interaction at the Oceanic Mesoscale, In Annual Review of Marine Science (Vol. 8), https://doi.org/10.1146/annurev-marine-010814-015606, 2016.

Molemaker, M. J., McWilliams, J. C., and Dewar, W. K.: Submesoscale generation of mesoscale anticyclones near a separation of the California Undercurrent, J. Phys. Oceanogr., 45, 613-629, https://doi.org/10.1175/JPO-D-13-0225.1, 2015.

Mouriño-Carballido, B., and McGillicuddy, D. J.: Mesoscale variability in the metabolic balance of the Sargasso Sea, Limnol. Oceanogr., 51(6), 2675-2689, https://doi.org/10.4319/lo.2006.51.6.2675, 2006.

Mouriño-Carballido, B.: Eddy-driven pulses of respiration in the Sargasso Sea, Deep-Sea Res. I: Oceanogr. Res. Pap., 56(8), 1242-1250, https://doi.org/10.1016/j.dsr.2009.03.001, 2009.

Mühlenbruch, M., Grossart, H. P., Eigemann, F., and Voss, M.: Mini-review: Phytoplankton-derived polysaccharides in the marine environment and their interactions with heterotrophic bacteria. Environ. Microbiol., 20(8), 2671–2685. https://doi.org/10.1111/1462-2920.14302, 2018.

Neijssel, O. M., and Mattos, M. J. T. De.: Micro Review The energetics of bacterial growth : a reassessment, 13(2), 179-182, 1994.

Nielsen, E. S.: The use of radio-active carbon (c14) for measuring organic production in the sea, ICES Mar. Sci., 18(2), 117-140, https://doi.org/10.1093/icesjms/18.2.117, 1952.

Noyon, M., Morris, T., Walker, D., and Huggett, J.: Plankton distribution within a young cyclonic eddy off south-western Madagascar, Deep Sea Res. Part II Top. Stud. Oceanogr., 166, 141-150, https://doi.org/10.1016/j.dsr2.2018.11.001, 2019.

Obernosterer, I., and Herndl, G. J.: Phytoplankton extracellular release and bacterial growth: Dependence on the inorganic N:P ratio. Mar. Ecol. Prog. Ser., 116, 247–258, https://doi.org/10.3354/meps116247, 1995.

Pegliasco, C., Chaigneau, A., and Morrow, R.: Main eddy vertical structures observed in the four major Eastern Boundary Upwelling Systems. J. Geophys. Res. Oceans, 120(9), 6008–6033, https://doi.org/10.1002/2015JC010950, 2015.

Pelegrí, J. L. and Peña-Izquierdo, J.: Eastern boundary currents off North-West Africa. In: Oceanographic and biological features in the Canary Current Large Marine Ecosystem. Valdés, L. and Déniz-González, I. (eds). IOC- UNESCO, Paris. IOC Technical Series, No. 115, pp. 81-92, URI: http://hdl.handle.net/1834/9179, 2015

Piontek, J., Endres, S., Le Moigne, F. A. C., Schartau, M., and Engel, A.: Relevance of Nutrient-Limited Phytoplankton Production and Its Bacterial Remineralization for Carbon and Oxygen Fluxes in the Baltic Sea. Front. Mar. Sci., 6, 1–16, https://doi.org/10.3389/fmars.2019.00581, 2019.

Rao, D. N., Chopra, M., Rajula, G. R., Durgadevi, D. S. L., and Sarma, V. V. S. S.: Release of significant fraction of primary production as dissolved organic carbon in the Bay of Bengal, Deep Sea Res. Part I Oceanogr. Res., 168, 1-27, https://doi.org/10.1016/j.dsr.2020.103445, 2021.

Regaudie-De-Gioux, A., and Duarte, C. M.: Temperature dependence of planktonic metabolism in the ocean. Glob. Biogeochem. Cycles, 26(1), GB1015, https://doi.org/10.1029/2010GB003907, 2012.

Reinthaler, T., Bakker, K., Manuels, R., van Ooijen, J., and Herndl, G. J.: Erratum to Fully automated spectrophotometric approach to determine oxygen concentrations in seawater via continuous-flow analysis. Limnol. Oceanogr. Methods 5(1), 72–72. https://doi.org/10.4319/lom.2007.5.72, 2006.

Robinson C.: Heterotrophic bacterial respiration. In: Kirchman DL (ed) Microbial ecology of the oceans, Wiley-Liss, New York, NY., 2008.

Russell, J. B. and Cook, M. G.: Energetics of Bacterial Growth : Balance of Anabolic and Catabolic Reactions, Microbiol Rev., 59(1), 48-62, 1995.

Schlitzer, R.: Ocean Data View, odv.awi.de, 2020.

Schütte, F., Brandt, P., and Karstensen, J.: Occurrence and characteristics of mesoscale eddies in the tropical northeastern Atlantic Ocean, Ocean Sci., 12, 663-685, https://doi.org/10.5194/os-12-663-2016, 2016.

964   Simon, M., and Azam, F.: Protein content and protein synthesis rates of planktonic marine
965   bacteria, Mar. Ecol. Prog. Ser., 51, 201-213, 1989.

966   Singh, A., Gandhi, N., Ramesh, R., and Prakash, S.: Role of cyclonic eddy in enhancing
967   primary and new production in the Bay of Bengal, J. Sea Res, 97, 5-13,
968   https://doi.org/10.1016/j.seares.2014.12.002, 2015.

969   Smith, D., and Azam, F.: A simple, economical method for measuring bacterial protein
970   synthesis rates in seawater using. Mar. Microb. Food Webs, 6(2), 107-114, 1992.

971   Solórzano, L.: Determination of Ammonia in Natural Waters by the Phenolhypochlorite
972   Method, Limnol. Oceanogr., 14, 799-801, 1969.

973   Strickland, J.D.H. and Parsons, T.R.: A Practical Handbook of Seawater Analysis. Bulletin
974   of Fisheries Research Board of Canada, 167, 1-311, 1968.

975   Thomsen, S.: The formation of a subsurface anticyclonic eddy in the Peru-Chile
976   Undercurrent and its impact on the near-coastal salinity, oxygen, and nutrient distributions,
977   J. Geophys. Res. Oceans, 121, 476-501, https://doi.org/ 10.1002/2015JC010878, 2016.

978   Vaqué, D., Alonso-Sáez, L., Arístegui, J., Agustí, S., Duarte, C. M., Montserrat Sala, M.,
979   Vázquez-Domínguez, E., and Gasol, J. M.: Bacterial production and losses to predators
980   along an Open ocean productivity gradient in the Subtropical North East Atlantic Ocean. J.
981   Plankton Res., 36(1), 198-213, https://doi.org/10.1093/plankt/fbt085, 2014.

982   Wear, E. K., Carlson, C. A., and Church, M. J.: Bacterioplankton metabolism of
983   phytoplankton lysates across a cyclone-anticyclone eddy dipole impacts the cycling of
984   semi-labile organic matter in the photic zone, Limnol. Oceanogr., 65(7), 1608-1622,
985   https://doi.org/10.1002/lno.11409, 2020.

986   Wickham H.: tidyverse: Easily Install and Load 'Tidyverse' Packages. See https://cran. r-
987   project.org/package=tidyverse, 2016.

988   Wilhelm, W. L.: Die Bestimmung des im Wasser gelösten Sauer- stoffes, Ber. Dtsch. Chem.
989   Ges., 21, 2843-2854, 1888.

990   Xu, G., Dong, C., Liu, Y., Gaube, P., and Yang, J.: Chl a Rings around Ocean Eddies in the
991   North Pacific, Sci. Rep., 9(1), 1-8, https://doi.org/10.1038/s41598-018-38457-8, 2019.

992